Title: Transcriptomic and exometabolomic profiling reveals antagonistic and defensive modes of *Clonostachys rosea* action against *Fusarium graminearum*

Zerihun A. Demissie[1], Thomas Witte[2], Kelly A. Robinson[1], Amanda Sproule[2], Simon J. Foote[3], Anne Johnston[2], Linda J. Harris[2], David P. Overy[2] and Michele C. Loewen[1,4,5*]

[1]Aquatic and Crop Resource Development, National Research Council of Canada, Ottawa, ON, Canada

[2]Ottawa Research and Development Centre, Agriculture and Agri-Food Canada, Ottawa, ON K1A 0C6, Canada

[3]Human Health Therapeutics, National Research Council of Canada, Ottawa, ON, Canada

[4]Department of Biomedical and Molecular Sciences, Queens University, Kingston, ON, Canada

[5]Department of Chemistry and Biomolecular Sciences, University of Ottawa, Ottawa, ON, Canada

*** Corresponding Author:** Michele C. Loewen; Email: michele.loewen@nrc.ca

ABSTRACT:

The mycoparasite *Clonostachys rosea* strain ACM941 is under development as a bio-control organism against *Fusarium graminearum,* the causative agent of Fusarium Head Blight in cereals. To identify molecular factors associated with this interaction, the transcriptomic and exometabolomic profiles of *C. rosea* and *F. graminearum* strain GZ3639 were compared during co-culture. Prior to physical contact, the antagonistic activity of *C. rosea* correlated with a response heavily dominated by up regulation of polyketide synthase gene clusters, consistent with the detected accumulation of corresponding secondary metabolite products. Similarly, prior to contact, trichothecene gene clusters were upregulated in *F. graminearum,* while those responsible for fusarielin and fusarin biosynthesis were downregulated; correlating with an accumulation of trichothecene products in the interaction zone over time. A concomitant increase in 15-acetyl deoxynivalenol-3-glucoside in the interaction zone was also detected, with *C. rosea*

established as the source of this detoxified mycotoxin. After hyphal contact, *C. rosea* was found to predominantly transcribe genes encoding cell wall degradation enzymes, major facilitator superfamily sugar transporters, anion:cation symporters as well as alternative carbon source utilization pathways, together indicative of a transition to necrotropism at this stage. *F. graminearum* notably activated the transcription of phosphate starvation pathway signature genes at this time. Overall, a number of signature molecular mechanisms likely contributing to *C. rosea*'s antagonistic activity against *F. graminearum,* as well as its mycotoxin tolerance, are identified in this report, yielding several new testable hypotheses toward understanding the basis of *C. rosea* as a bio-control agent for continued agronomic development and application.

KEY WORDS: antagonism, biocontrol agent, *Clonostachys rosea*, deoxynivalenol, detoxification, *Fusarium graminearum,* glycosylation, polyketides

ABBREVIATIONS: 15-acetyl-deoxynivalenol, 15-ADON; 15-acetyl-deoxynivalenol-3-glycoside, 15-ADON-3-Glc; acetonitrile, ACN; after contact, AC; before contact, BC; deoxynivalenol, DON; droplet digital polymerase chain reaction, ddPCR; fusarium head blight, FHB; major facilitator superfamily, MFS; mass to charge ratio, *m/z*; methanol, MeOH; polyketide synthase, PKS; quantitative polymerase chain reaction, qPCR; retention time, RT; ultra-high performance liquid chromatography- high resolution mass spectrometer, UPLC-HRMS; zearalenone, ZEA.

INTRODUCTION

The genus *Clonostachys rosea* (Schroers *et al.*, 1999) includes a number of endoST1Tphytic soil-borne ascomycete strains recognized for their ability to promote plant growth and/or to protect crop yields from pathogens and mycotoxin contamination. Some of the plant pathogens reportedly controlled by *C. rosea* include *Fusarium* spp., *Alternaria* spp., *Botrytis* spp. and *Pythium tracheiphilum* (Lysøe et al. 2017; Sutton et al. 1997; Zhang et al. 2008). The *C. rosea* strain ACM941, isolated from pea plants in Manitoba, Canada in 1994 (Hue et al. 2009), is a biocontrol agent patented for use against *Fusarium graminearum* (Xue 2002). *F. graminearum* is the leading cause of Fusarium Head Blight (FHB) in North America and *C. rosea* has been shown to reduce the FHB index by 46 % and deoxynivalenol (DON) levels by 33 % compared to controls (Xue et al. 2014). However, the molecular basis of its necrotrophic mycoparasitism against *F. graminearum* and its mycotoxin tolerance have remained largely enigmatic.

Experimental evidence and comparative genome analyses indicate that secondary metabolites play a central role in *C. rosea* mycoparasitism (Karlsson et al. 2015, 2017). For example, fifteen secondary metabolites were isolated from *C. rosea* strain YRS-06 of which tetrahydrotrichodimer ether, dihydrotrichodimer ether A, dihydrotrichodimer ether B, TMC-151C and TMC-151E displayed promising antibacterial activity (Zhai et al. 2016). As well, *Sclerotiania sclerotiorum* growth inhibitory molecules, mainly composed of non-ribosomal peptides, were also characterized from *C. rosea* strain BAFC3874 (Rodríguez et al. 2011). A recent study also showed that deletion of a non-ribosomal peptide synthase gene (*NRPS1*) significantly weakens *C. rosea* strain IK726 nematicidal property and its' *in planta* biocontrol activity against foot rot disease caused by *F. graminearum* (Iqbal et al. 2019). With respect to

FHB, *C. rosea* strain ACM941 secretes *F. graminearum* growth inhibitory molecules and predicted associated biosynthetic gene clusters were described (Demissie et al. 2018).

Additionally, *C. rosea* likely employs cell wall degrading enzymes to facilitate necrotrophism. Mycoparasitism of *Botrytis allii* by *C. rosea* was attributed to both low molecular weight secreted metabolites and cell wall degrading enzymes in particular β-(1,3)-glucanases and chitinases (Pachenari and Dix 1980). Scanning and transmission electron microscopy images of *C. rosea* interacting with *B. cinerea* (Yu and Sutton 1997; Li et al. 2002) also showed penetration of the *B. cinerea* hyphae by *C. rosea,* presumably enabled by enzymatic degradation, leading to cytoplasmic organelle disintegration. The cell wall degrading enzyme associated with the endochitinase gene Chi67-1 (isolated from *C. rosea* strain 67-1; (Sun et al. 2015)) has been functionally characterized and directly linked to *C. rosea*'s biocontrol property. Contrary to this, deletion of a pectate lyase gene PEL12 in strain IK726 failed to attenuate its mycoparasitic activity against *B. cinerea* (Atanasova et al. 2018). These mixed results highlight that the antagonistic mode of *C. rosea* is complex, likely involving both secondary metabolites and cell wall degrading enzymes.

Mycotoxin tolerance is an important trait of mycoparasitisizing organisms, to enable their survival and neutralize toxigenic fungal defense metabolites. Transcriptomic profiling (Kamou et al. 2016; Kosawang et al. 2014;), gene deletion experiments (Dubey et al. 2014) and comparative genomic analysis (Karlsson et al. 2015, 2017) of *C. rosea* have suggested that mycotoxin tolerance in *C. rosea* is likely a result of ATP-binding cassette (ABC) transporter-mediated efflux. In this regard, *C. rosea* grown in medium amended with fumonisin B1 showed no sign of growth retardation, or any evidence of degraded or detoxified fumonisin B1, leading to the conclusion that its tolerance involves cellular clearance likely by ABC transporter proteins

(Chatterjee et al. 2016). In addition, expression of the ABC-transporter gene *pdr5* increased upon *C. rosea* strain IK726 exposure to zearalenone (ZEA) (Kosawang et al. 2014) and *pdr5* deletion reduced ZEA tolerance (Dubey et al. 2014). Similarly, deletion of *pdr5* or mutations of key residues in its active site weakened yeast tolerance towards DON type mycotoxins (Gunter et al. 2016). However, evidence suggests that enzymatic activity may also play a role in mycotoxin detoxification by *C. rosea*. For example, despite the evidence suggesting that *C. rosea* IK726 tolerance towards ZEA is mediated by PDR5 (Dubey et al. 2014; Kosawang et al. 2014), its detoxification was previously shown to be catalyzed by the ZEA hydrolase enzyme ZHD101 (Takahashi-Ando et al. 2002). Similarly, although a 33% reduction in DON levels has been achieved by *C. rosea* strain ACM941 in field and greenhouse experiments (Xue et al. 2014), it is not known if this is a result of *F. graminearum* growth inhibition or DON detoxification or both.

Toward addressing these gaps in our understanding of the mechanisms underlying the biocontrol activity of *C. rosea* strain ACM941 against *F. graminearum* strain GZ3639, as well as its trichothecene tolerance, an experimental co-culturing system using plate confrontation assays was set up to compare both secondary metabolite excretion and gene transcription between inter-acting species and monoculture controls. Presented here are the results of transcriptomic and metabolomics profiling analyses that were used to compare the interspecies responses during confrontation, both 'before contact' (BC) and 'after contact' (AC). The upregulation of secondary metabolite gene cluster expression and resulting metabolite accumulation in the interaction zone were found to occur BC, followed by a transition to necrotrophic growth and associated enzymatic expression of *C. rosea* AC. Together these findings highlight signature molecular mechanisms underlying the antagonistic effects and mycotoxin tolerance of *C. rosea*, raising an array of novel hypotheses for future testing and application to agricultural agronomy.

RESULTS

Phenotypic evaluation of the *C. rosea* and *F. graminearum* colony confrontation

Fungal confrontation experiments showed that the mycelium growth of the *F. graminearum* edge directly opposing the *C. rosea* growing edge slowed down significantly after 5 days of co-culture. Instead, the *F. graminearum* leading edge was found to be growing vertically and laterally. In contrast, *C. rosea* grew steadily before reaching the *F. graminearum* edge and continued to grow over it.

C. rosea and *F. graminearum* RNAseq analysis and validation

Two reference genomes of *C. rosea* – strain IK726 (Karlsson et al. 2015) and strain CBS125111 (http://genome.jgi.doe.gov/pages/search-for-genes.jsf?organism=Cloro1) and a *de novo* assembled transcript database of strain *C. rosea* strain ACM941 are available (Demissie et al. 2018). In this report, the IK726 genome derived transcripts were used as a reference for transcript abundance quantification for two purposes: to be consistent with a recently reported similar study (Nygren et al. 2018) and to compare the response of the two strains. Of the 14,628 *C. rosea* transcripts, 1,145 transcripts were differentially regulated in *C. rosea* (with ≥ 2.0 fold expression, p-value <0.05), with 561 down and 584 upregulated, respectively, before the two mycelia made contact (BC) (Fig. **1A**). The number of differentially regulated *C. rosea* transcripts after the *C. rosea* and *F. graminearum* mycelia made contact (AC) was 2,082 (with ≥ 2.0 fold expression, p-value <0.05), of which 940 were downregulated and 1,142 were upregulated (Fig. **1B**). On the other hand, RNASeq analysis of *F. graminearum* co-cultured with *C. rosea* revealed 864 and 882 genes were down and upregulated BC greater than two-fold, respectively, compared to the control (p-value <0.05), while 1,009 and 765 genes were down and upregulated AC, respectively (Table S1).

To confirm the veracity of the RNAseq expression data, qPCR primers were designed against candidate *C. rosea* transcripts whose expression was either not changed, upregulated or downregulated in one or both stages (Table S2). With the exception of *BN869_T00007232_1*, whose transcript abundance remained unchanged in the AC RNA sample using qPCR, the RNAseq expression profiles of all transcripts correlated well with those arising from qPCR (Fig. **2**). Therefore, the RNAseq analysis results were deemed sufficiently reliable to represent the biological events occurring during the *C. rosea* and *F. graminearum* interaction, and were advanced for further detailed analysis. Similarly, selected *TRI* (trichothecene) genes were used to validate RNAseq results of *F. graminearum* using ddPCR and were also found to corroborate the expression data (Fig. **3, S1**).

On the assumption that *C. rosea* mycoparasitism against *F. graminearum* is likely determined by upregulated transcripts, the remaining analysis was largely focused on these groups. A total of 361 (Table **S3**) and 638 (Table **S4**) transcripts showed significant up regulation BC and AC (with ≥ 2.5 fold expression at p-value <0.05), respectively, of which only 52 were common (Table S5). This lack of transcript commonality suggests divergence in *C. rosea's* response at the BC and AC stages. This was further supported by the distribution of GO terms associated with transcripts upregulated at the BC and AC stages. In particular, 24 (6%) transcripts with GO terms related to small metabolite biosynthesis were upregulated at the BC stage, while only 5 (<1%) transcripts with similar GO terms were upregulated ≥ 2.5 fold in *C. rosea* AC (Fig. S3). This implies that secondary metabolism biosynthesis is initiated early on in the interaction, likely involving both "first line" offensive and defensive mechanisms from *C. rosea*. Further investigation of the expression of the top 100 upregulated transcripts from each time point (BC and AC), of which only 10 were in common, further emphasized this (Fig. **4A**;

Tables **S2, S3**). Notably, cell wall degrading enzymes were substantially upregulated AC, while polyketide synthase homolog transcripts were detected BC, with details presented below. Together these findings underscore a substantial change in the type of transcripts being upregulated at the two stages, and suggest that *C. rosea*'s mode of antagonism shifts depending on its proximity to *F. graminearum*. A similar effect was observed for *F. graminearum,* with only 5 of the top 100 upregulated genes, putatively encoding glutathione S-transferase, cytochrome b-5 reductase and hypothetical proteins, upregulated in both stages of the interaction (Fig. **4B**; Table S1).

Extracellular metabolite accumulation validates *C. rosea* and *F. graminearum* in 'Before Contact' signature secondary metabolite gene cluster expression

Three gene clusters with putative roles in secondary metabolite biosynthesis were upregulated in *C. rosea* co-cultured with *F. graminearum* at the BC stage (Table **S3**). Two of these clusters were anchored by polyketide synthase homolog transcripts including *BN869_T00012010_1* that was expressed ~16 fold higher (Fig. **5**), *BN869_T00013405_1* expressed 4.2 fold higher, and *BN869_T00010693_1* and *BN869_T00010694_1* expressed 2.2 and 2.6 fold higher, respectively (Table **1**). qPCR analysis of these genes validated their RNAseq expression (Fig. **5** and data not shown). Notably, transcripts *BN869_T00010693_1* and *BN869_T00010694_1* putatively encode homologs of a highly reducing polyketide synthase (77% similarity) and a non-reducing polyketide synthase (78% similarity) respectively. These were identified by BLAST analysis against the UniProt database and FungiSMASH search as SorB and SorA homologs of the bisorbicillinoids gene cluster, respectively (Guzmán-Chávez et al. 2017). Other members of the gene cluster were similarly upregulated (Table **1**). The gene cluster anchored by the polyketide homolog *BN869_T00012010_1* (Fig. **5**) also contained

epoxide hydrolase, asparagine synthase and cytochrome p450 encoding transcripts, along with two transcripts with unknown function that were also upregulated. A third potential secondary metabolism related gene cluster upregulated at the BC stage was anchored by the major facilitator superfamily (MFS) transporter protein homolog *BN869_T00007234_1* that was upregulated 125 fold (Fig. **2**). However, although neighboring genes were also upregulated, fulfilling a gene cluster category criteria, a putative function for this cluster cannot be assigned at this time.

While, the *C. rosea* genome is not sufficiently well annotated to enable informed gene function predictions, in comparison, the *F. graminearum* genome is very well annotated, enabling prediction and correlation of differentially regulated gene clusters with metabolites. Sieber *et al.*, (2014) had identified 67 predicted secondary metabolism gene clusters (C01 to C67) by combining functional enrichment analysis of the *F. graminearum* genome with supporting co-expression data. RNAseq expression data of *F. graminearum* challenged by *C. rosea* showed that 15 of the 67 gene clusters were significantly differentially regulated between treatments (Supplemental Table S6). Gene clusters responsible for biosynthesizing the fusarielins (C60; Sørensen *et al.*, 2012), fusarins (C42; Niehaus *et al.*, 2013), malinochrome (C63; Oide et al 2015) and an unknown metabolite possibly related to iron transport (C22) were all downregulated at the BC stage. In addition, at least a subset of genes within the uncharacterized clusters C06 (containing *NRPS16*, *NRPS19*) and C07 were also downregulated at BC. In contrast, the trichothecene (C23; Fig. 3) (as well as the unlinked *TRI1* and *TRI101* genes), zearalenone (C15), aurofusarin (C13; Frandsen et al., 2011) gene clusters and the two culmorin biosynthetic genes were upregulated in the BC samples while the gramillin gene cluster (C02;

Bahadoor *et al.*, 2018) was upregulated both BC and AC. Two gene clusters, C28 (carotenoid, Jin et al. 2010) and the uncharacterized C25, were downregulated after contact with *C. rosea*.

To validate the differential expression of the above gene clusters with their predicted secreted metabolites, the exometabolites of *C. rosea* and *F. graminearum* isolated from co-cultured plates compared to that of their respective mono-culture conditions were profiled. Data preprocessing yielded a total of 140 variables (representing pseudomolecular ions) that were detected above thresholding limits. The data was modelled by PCA to check for sample outliers, showing clear separation between the 4 different sample classes in the first two principle components and explaining the majority of the variance in the model (Fig. S4). A correlation analysis was performed to group associated pseudomolecular ion variables (protonated mass, adducts, neutral losses, fragments) based on expression levels and retention times; reducing the complexity of the data set down to 70 variable groupings. Pairwise comparisons were carried out on representative variables between monoculture and associated co-culture interaction-zone data sets, yielding a specific list of variables with significant differences in fold change (p-value < 0.05) associated with differential metabolite accumulation in the interaction zone at all time points during the time course. The greatest amount of observed variance in secreted metabolite accumulation occurred between sample classes in those extracted from agar plugs harvested after the two colonies made contact. All AC samples were subjected to a cluster analysis and an associated heat map of log-scaled metabolite accumulation was generated to visualize and compare trends in metabolite accumulation occurring between the monocultures and within the co-culture interaction zones (Fig. **6**). Exometabolites in the monoculture strains formed two clearly distinct clades, emphasizing the lack of overlapping metabolite expression/secretion by *C. rosea* and *F. graminearum*. At the same time, metabolite production from the interaction

zones consisted of a mixture of metabolites observed from the two monoculture strains, along with variables that were unique to the interaction zone and absent from monoculture strains.

Annotations were possible for a number of *C. rosea* secondary metabolites based on published data (Zhai et al. 2016). Trichodimerol and associated bisorbicillinoid analogs (such as dihydro- and tetrahydrotrichodimer ethers) as well as the polyketides TMC-151A, TMC-151C,TMC-151E and other associated analogs were observed in *C. rosea* monoculture secreted metabolite profiles and *C. rosea* - *F. graminearum* interaction zones. Based on pseudomolecule ion peak area, relative accumulation levels were found to steadily increase over the experimental time course as cultures matured, diffusing through the agar from *C. rosea* to *F. graminearum* in the confrontation zone (Fig. **7A-D**). Fluctuations in secondary metabolite production were also observed in *F. graminearum* monocultures compared to *C. rosea* - *F. graminearum* co-cultures. Accumulation of fusarin, 15-acetyl-deoxynivalenol (15-ADON) and other associated trichothecenes were observed in *F. graminearum* monocultures at the AC stage (i.e. by day 7), confirming their production from *F. graminearum*. Significant fold changes in 15-ADON accumulation were observed in the interaction zone of the co-cultures compared to *F. graminearum* monocultures at sampling time points both BC and AC, as predicted by BC differential *TRI* gene expression observed in the transcriptomic analyses (Fig. **3, S1**). Differential production of ZEA, culmorin, and aurofusarin as suggested by the RNAseq data (Table **S6**) was confirmed by extracted ion chromatograms of the UPLC-HRMS profiles to occur AC in the co-culture interaction zones adjacent to *F. graminearum* compared to *F. graminearum* monocultures (and absent in *C. rosea* monocultures). Gramillin-associated pseudomolecular ion signals were not detected by UPLC-HRMS profiling, despite up regulation of its gene cluster

(Table **S6**), which is likely an artifact of the extraction process as gramillins are not soluble in ethyl acetate.

C. rosea detoxifies 15-ADON by glycosylation

The mycotoxin tolerance observed in ACM941 and other *C. rosea* strains has been attributed to active efflux via ABC transporter proteins (Dubey et al. 2014; Karlsson et al. 2015). Therefore, the detection of 15-ADON-3-*O*-glucoside (15-ADON-3-Glc) in the *C. rosea* and *F. graminearum* confrontation zone of co-culture plates was unexpected (Fig. **6, 8**). Indeed, 15-ADON-3-Glc was absent in both of the monoculture controls over the duration of the time course. Confirmation of the identification of 15-ADON-3-Glc was carried out by MS/MS experiments, where pseudomolecular fragment ions matched those of published data (Schmeitzl et al. 2015). Similar to 15-ADON, 15-ADON-3-Glc increased steadily in abundance over the time course in the confrontation zone, initiated BC, with concentrations consistently greatest at the *C. rosea* colony periphery, compared to that of *F. graminearum*. Taken together, these accumulation patterns suggest that while 15-ADON was secreted by *F. graminearum* and diffused towards the *C. rosea* periphery, it is transformed to 15-ADON-3-Glc by *C. rosea* which subsequently diffuses back across the confrontation zone. In a separate experiment, when *C. rosea* was challenged with differing concentrations of pure 15-ADON, production of 15-ADON-3-Glc through glycosylation of 15-ADON by *C. rosea* was confirmed (Fig. S5), albeit glycosylation occurred at a lesser extent than observed in the confrontation plates. This data raises the novel hypothesis that the 15-ADON glycosylation reaction is mediated by an endogenous glycosyltransferase from *C. rosea*, whose up regulation may involve dynamic signals arising from the *F. graminearum* secretome.

C. rosea triggers expression of cell wall degradation and enhanced competitive fitness related transcripts 'After Contact' with *F. graminearum*

Cell wall degradation is part of *C. rosea's* necrotrophic mycoparasitism as shown in interactions with *B. cinerea* (Li et al. 2002). *C. rosea* is also predicted to exploit similar mechanisms against *F. graminearum*, although this has not been described to date. To address this hypothesis, putative functions were assigned to significantly upregulated *C. rosea* transcripts at the AC stage to identify those encoding possible cell wall degradative enzymes (Table **2**). Twelve cell wall degrading and three proteolytic enzyme encoding homolog transcripts were found to be differentially regulated in *C. rosea* co-cultured with *F. graminearum* either BC or AC. A β-galactosidase and β-1,2-glycosyl hydrolase family 61 homologs were significantly expressed at the BC stage while the α-β hydrolase homolog *BN869_T00014078_1* was upregulated at both the BC and AC stages, but prominently expressed at BC stage. Eight glycoside hydrolase homologs were significantly upregulated after the *C. rosea* periphery merged with that of *F. graminearum*. Protease homologs were the second most upregulated *C. rosea* transcripts potentially involved in *C. rosea*'s antagonistic activity after colony contact (Table **2**). To validate these results, the expression profile of *BN869_T00010437_1* was tested using qPCR and found to correlate well with the RNAseq data (data not shown).

Genes associated with a response to phosphate starvation were upregulated in *F. graminearum* in the presence of *C. rosea* (Table **3**). For example, a *BTA1* homolog was one of the most prominently induced genes before the *F. graminearum* growing edge merged with that of *C. rosea*. *BTA1* encodes an enzyme known to contribute to the biosynthesis of phosphorus-free betaine lipids (Riekhof et al. 2014). Under conditions of phosphate limitation, betaine lipids can be produced to replace phosphatidylcholine in membranes to conserve phosphate for other

essential cell processes. Further to this, other genes potentially impacted by phosphate limitation were found to be differentially expressed (Table **3**). In yeast, the high-affinity phosphate transporter PHO84 and secreted acid phosphatases are induced under phosphate-limiting conditions (Lenburg and O'Shea 1996). Interestingly the *FGRAMPH1_01G25919* encoding a protein exhibiting 55% amino acid identity to PHO84 was induced in the presence of *C. rosea*. Two genes, distantly related to secreted acid phosphatase yeast PHO5, were both upregulated, along with three other genes encoding acid phosphatases. PHO89 is a sodium/phosphate co-transporter, localized to the plasma membrane, with the protein product of *FGRAMPH1_01G08015* sharing 42% amino acid identity with PHO89 and is induced 3-fold in the presence of *C. rosea*. Yeast GIT1 is a plasma membrane transporter importing glycerol-3-phosphate and phospholipids and regulated by the availability of phosphate and inositol (Almaguer et al. 2003). *FGRAMPH1_01G13431* is related (E = 4.6e-77) to *GIT1* and upregulated 4-fold after *C. rosea* confrontation. Phosphate can also be liberated by lipid phosphatidate phosphatase, for which a homolog was induced BC. The induction of these genes involved in non-phosphorus membrane biosynthesis and phosphate transport is similar to expression profiles exhibited during *F. graminearum* infection of maize stalks, which also provides an environment limited in phosphate (Zhai et al. 2016). Expression profiles of *FGRAMPH1_01G01877*, *FGRAMPH1_01G25919* and *FGRAMPH1_01G15463* detected by RNAseq were validated by ddPCR (Fig. S2).

The expression of available corresponding *C. rosea* homologs was also evaluated, but only *BN869_T00007330_1* (lipid phosphatidate phosphatase, homolog of *FGRAMPH1_01G12109*) was differentially expressed, with 17-fold (Padj < 2.47E-25) and 6-fold (Padj < 2.49E-80) induction respectively BC and AC, during co-culture. This suggests that

C. rosea is not experiencing phosphate limitation to the same extent as *F. graminearum* during the fungal competition.

Differentially regulated *C. rosea* transcripts were explored to identify mechanisms possibly involved in alleviating similar phosphate starvation and other nutritional scarcity related stress responses. The analysis revealed that in the confrontation with *F. graminearum*, *C. rosea* enhances its competitiveness in part by expanding its carbon source repertoire, by induction of the ethanol utilization pathway (Flipphi et al. 2003, 2006), as well as redirecting terpene precursors back to the TCA cycle through the mevalonate shunt pathway (Rodríguez et al. 2004). The ethanol utilization pathway (alc system) of *Aspergillus nidulans* includes alcohol dehydrogenase (*alcA)*, aldehyde dehydrogenase (*aldA)*, and a regulatory gene (*alcR)*. Putative *C. rosea alcS*, *alcA*, *aldA* and *alcR* transcripts were all upregulated after the *C. rosea* growing edge contacted that of *F. graminearum* (Table **S7**). The concurrent up regulation of the *alc* pathway with several glycosyl hydrolases after the two fungi make physical contact is also notable. Two transcripts located upstream of *alcA*, putatively encoding acetyl_CoA synthetase and an unknown protein were also upregulated. In addition, a cation transporting ATPaseI homolog, methylcrotonyl CoA carboxylase α and β subunits, and two transcripts showing low homology to hydratases residing downstream of the *alc* pathway homolog transcripts were also upregulated. Methylcrotonyl CoA carboxylase α and β subunits along with *alcA, aldA* and hydratases are involved converting the isoprenoid pathway general precursors into acetyl-CoA through the "mevalonate shunt" pathway (Brady et al. 1982).

Differential regulation of *C. rosea* major facilitator superfamily transporter homolog transcripts

MFS are ubiquitous membrane transporter proteins involved in substrate translocation across cell membranes (Gbelska et al. 2006). A total of 63 unique *C. rosea* MFS homolog transcripts were upregulated at the BC and/or AC stages of which 20 were exclusively expressed at BC and 39 at AC. Four transcripts were upregulated at both stages. In a previous study, MFS homolog transcripts were among the most upregulated transcripts 24 hours after *C. rosea* strain IK726 mycelium made contact with that of *F. graminearum* strain PH-1 (Nygren et al. 2018). In our study, of the 22 MFS homologs upregulated in IK726 interacting with PH-1, only six were significantly upregulated in *C. rosea* (strain ACM941) co-cultured with *F. graminearum* (strain GZ3639) (Table **S8**). Of the six transcripts in common, *BN869_T00007234_1* was upregulated both BC and AC while others were upregulated only AC (Table 4). This transcript was the most upregulated transcript in IK726 co-cultured with PH-1 and a homolog of this was the second most upregulated transcript in *C. rosea* (strain ACM941) interacting with *F. graminearum* (strain GZ3639). As shown in Fig. **2**, transcript *BN869_T00007234_1* was upregulated as part of a gene cluster which included transcripts showing homology to NADPH dehydrogenase, hydrolase, acetamidase and a transcription factor.

According to the Transporter Classification Database (TCDB) (Saier et al. 2016), proteins included in the MFS family were classified into different subfamilies based on their sequence homology and conserved function. The main upregulated MFSs in *C. rosea* belong to subfamily 2.A.1.1 – sugar transporters, 2.A.1.2 – the Drug:H+ Antiporter-1 (DHA1), 2.A.1.3 – the Drug:H+ Antiporter-2 (DHA2), 2.A.1.13 – monocarboxylate transporters and 2.A.1.14 – the anion:cation symporters. Upregulated *C. rosea* MFSs classified as sugar transporters, DHA2 and anion:cation symporters were either upregulated at the BC or AC stages compared to the other subfamilies. For example, 13 out of 17 transcripts belonging to the family of sugar porter

subfamily were exclusively upregulated in *C. rosea* AC with *F. graminearum* while 2 were upregulated both BC and AC (Table 4). In addition, 12 of the 15 symporters that use organic anions as substrates including cell wall degradation products were upregulated AC. It is notable that, the expression of these transcripts correlated well with the expression of cell wall degrading enzyme homolog transcripts (Table **2**). This, coupled with the fact that phosphate starvation response genes were not significantly upregulated in C. rosea, as opposed to *F. graminearum* (Table **3**), indicates the competitive advantage of *C. rosea* over *F. graminearum* in this limited resource environment. Together these results raise another new hypothesis wherein *C. rosea* has increased competitive fitness in the later stage of the interaction, including uptake of nutrients released during degradation of *F. graminearum*.

In contrast, 8 of the 12 upregulated transcripts of the DHA2 subfamily were upregulated BC (Table 4). The DHA2 subfamily members are generally recognized for their mycotoxin efflux transport properties (Gbelska et al. 2006); therefore, the fact that their expression corresponds with the expression of secondary metabolite-related gene clusters (Fig. **5**) is notable. An approximately even number of transcripts belonging to the DHA1 subfamily were also upregulated, both BC and AC (3 and 5 transcripts, respectively).

DISCUSSION

Previously a concentration-dependent growth inhibition of *F. graminearum* strain GZ3639 by *C. rosea* strain ACM941 liquid culture filtrate was observed (Demissie et al. 2018), suggesting that *C. rosea* secretes secondary metabolites inhibitory to the growth of *F. graminearum*. This work corroborated previous reports (Rodríguez et al. 2011; Dubey et al. 2014) and comparative genomic study-based predictions (Karlsson et al. 2015, 2017). As *C. rosea* is a necrotrophic mycoparasite that can overgrow its prey, secretion of cell wall degrading

enzymes was also anticipated. Notably, microscopic studies have revealed that the destruction of *B. cinerea* by *C. rosea* is preceded by *C. rosea* coiling around or physically penetrating *B. cinerea* (Li et al. 2002; Yu and Sutton 1997). Together these reports imply that *C. rosea* utilizes both secreted secondary metabolites and cell wall degrading enzymes toward enabling its antagonistic activity. Consistent with this, the biochemical basis of *C. rosea* mycoparasitism against *B. allii* was reported to involve both toxin production and expression of cell wall degrading enzymes (Pachenari and Dix 1980). However, it is notable that signaling pathways activated in response to secreted molecules differ from those induced upon physical contact (Luo et al. 2017). This raises a hypothesis that responses from *C. rosea* to *F. graminearum* secreted signaling molecules differ from those arising from physical contact. Toward defining the specific contributions of the various molecular networks from a temporal perspective, the transcriptomic and exometabolomic responses of *C. rosea* co-cultured with *F. graminearum* were compared to their monoculture counterparts before and after inter-fungal contact.

Interestingly, only 41 transcripts were observed to be differentially regulated in *C. rosea* strain IK726 interacting with *F. graminearum* strain PH-1 (Nygren et al. 2018). This is in contrast, to the 7,847 transcripts that were differentially regulated when *C. rosea* ACM941 was co-cultured with *F. graminearum* strain GZ3639 at a similar interaction stage, described herein. In addition to inherent differences between the different strains and analysis methods used, it is also likely that the use of the minimal media Czapek Dox in the confrontation between IK726 and PH-1 may have influenced IK726's transcriptional response. In particular, secondary metabolite production related gene clusters are generally activated by nutrient stress (Keller 2019), potentially masking their differential expression. This was addressed herein by the use of nutrient rich media to minimize external stress in the interaction responses. As well, *C. rosea*

was grown for ten days before introducing *F. graminearum*, compared to the five days afforded to IK726. Prior incubation of *C. rosea* was required not only to account for its slow growing nature but also to mimic it's *in situ* biocontrol activity. *B. cinerea* control by *C. rosea* in raspberry tissue was superior when *C. rosea* was applied prior to pathogen inoculation and weakened significantly when inoculated at the time of pathogen inoculation or later (Yu and Sutton 1997). The slow growing habit of *C. rosea* could also be the result of its conspicuous secondary metabolite biosynthetic ability when competing for carbon sources (Fig. **6**). Consistent with this, *nrpS1* deletion mutants of IK726 were found to grow faster with more abundant conidiation compared to their wild type counterpart (Iqbal et al. 2019).

F. graminearum* secreted molecules induce secondary metabolite biosynthesis in *C. rosea

C. rosea and other similar biocontrol agents can use their chemical arsenal both to mediate beneficial effects on plants and to antagonize pathogenic organisms like *Fusarium spp*. However, this knowledge has been largely derived from gene expression profiling experiments or comparative genomics analysis of genes putatively encoding proteins involved in secondary metabolite biosynthesis, rather than direct investigations of the metabolites synthesized during the interaction (Demissie et al. 2018; Dubey et al. 2014; Karlsson et al. 2015). Consistent with observations from previous genetic studies, an accumulation of significantly greater amounts of distinct secondary metabolites were reported in the confrontation zone, along the periphery of both *C. rosea* and *F. graminearum* during co-culture (as compared to monocultures). Although most of the *C. rosea* extracellular metabolites produced in response to *F. graminearum* were not annotated, the polyketides trichodimerol /bisorbicillinoid analogs (Fig. **7A, B**) and TMC-151 related metabolites (Fig. **7C, D**) were among those produced in significantly higher amounts. Polyketides include a diverse array of natural products synthesized by the modular enzymes

called polyketide synthases (PKSs) and are hypothesized to play roles in *C. rosea* biocontrol activity. PKSs are some of the most enriched gene families in the *C. rosea* genome (Karlsson et al. 2015, 2017) and many polyketides have demonstrated antifungal properties (Kohno et al. 1999; Okuda et al. 2000; Zhai et al. 2016). For example, bisorbicillinoids are biosynthesized by gene clusters containing two polyketide synthases, reducing and non-reducing PKSs (Guzmán-Chávez et al. 2017), and have been isolated from biocontrol agents like *T. citrinoviride* (Evidente et al. 2009) and *C. rosea* strain YRS-06 (Zhai et al. 2016). Consistent with this, a putative *C. rosea* sorbicillinoid type gene cluster (identified by FungiSMASH) was found to be slightly upregulated before contact (Table **1**), consistent with the detection of bisorbicillinoid accumulation in the *C. rosea* colony periphery during co-culture (Fig. **7A, B**).

Exhibiting strong antimicrobial activity, TMC-151 related metabolites are thus far exclusive to *C. rosea* (Ju et al. 2007; Zhai et al. 2016). Certain TMC-151 and bisorbicillinoid analogs exhibited superior antibacterial activity compared to levofloxacin, erythromycin, streptomycin, ampicillin, and tetracycline against *E. coli*, *C. perfringens* and *B. subtilis* (Zhai et al. 2016). In the same study, culture broths of a *C. rosea* (strain YRS-06) were also found to have antifungal activity against several plant pathogens; however, a link between TMC-151 and bisorbicillinoid analogs and observed antifungal activities has yet to be tested. In this current study, the putative TMC-151 gene cluster reported previously from *C. rosea* strain ACM941 (Demissie et al. 2018) was not found to be upregulated BC or AC from *C. rosea* co-cultured colonies. One possible explanation of this variance is the time of sampling. In the previous study, upregulation of the proposed TMC-151 biosynthetic gene cluster was detected only 3 days after spore inoculation into liquid broth containing *F. graminearum* secretome metabolites (Demissie et al. 2018). Thus, most likely, sampling for the BC time point on day 5 in this current study was

too late to detect the transient induction of the previously proposed cluster. While the possibility that this is not in fact a TMC-151 biosynthetic gene cluster cannot be strictly eliminated, it is notable that no other suitable upregulated gene cluster presents itself as an alternative. A lack of correlation between observed transcript expression of a gene cluster and that of the resulting product accumulating is not uncommon in fungi (Okada et al. 2017).

When *F. graminearum* was confronted by *C. rosea*, the expression of fifteen secondary metabolite gene clusters was significantly affected. *TRI* gene expression and trichothecene biosynthesis increased (Fig. 3) as well as genes responsible for zearalenone and aurofusarin biosynthesis, while expression of genes responsible for fusarielin and fusarin biosynthesis decreased (Table S6). This is consistent with a previous report that showed that upregulation of trichothecences was accompanied by a decrease in other types of secondary metabolites derived from common precursors like acetyl CoA (Atanasova-Penichon et al. 2018). While many of the end products of gene clusters induced prior to contact exhibit antifungal activity (Medentsev et al 1993; Utermark and Karlovsky 2007), the upregulation of these gene clusters was not maintained after contact. Many of the differentially expressed gene clusters remain uncharacterized and some of the tailoring enzymes (e.g. cytochrome P450s, oxidoreductases, and glucosyltransferases) may be induced as part of a detoxification process.

C. rosea shifts its antagonistic mode to cell wall degradation after physical contact

Transcription of *C. rosea* genes encoding various cell wall degrading enzymes (Table **2**), support the hypothesis that cell wall degrading enzymes play a role in the necrotrophic and mycoparasitic nature of *C. rosea*. In this regard, enzymatic activity of β-(1,3)-glucanases and chitinases by *C. rosea* have been experimentally demonstrated (Pachenari and Dix 1980); however, to date only an endochitinase from *C. rosea* strain 67-1 has been shown to play a role

in its antagonism as a mycoparasite (Sun et al. 2017). In contrast, deletion of a pectate lyase gene that was enriched in *C. rosea* strain IK726 genome, did not affect its antagonism against *Fusarium spp* (Atanasova et al. 2018), perhaps due to the redundancy of cell wall degrading enzymes. In agreement with the findings reported by Pachenari & Dix (Pachenari and Dix 1980), the present study has shown that secondary metabolism related transcripts were upregulated BC between *C. rosea* and *F. graminearum,* while proteolysis and cell wall degradation related transcripts were mostly upregulated AC (Table **2**). These results imply that the *C. rosea* lifestyle transitions from secondary metabolite mediated antibiosis to prey destruction BC and AC with *F. graminearum,* respectively. In particular, proteolysis related enzymes like metalloproteases and peptidases, and cell wall degrading enzymes in the family of glucosyl hydrolases were upregulated AC. Similar types of proteolytic/cell wall degrading enzymes have been described to play a role during the necrotrophic stage of *Colletotrichum* plant pathogens (Gan et al. 2013; O'Connell et al. 2012).

Glycosylation plays a central role in *C. rosea* tolerance of 15-ADON

Tolerance of *C. rosea* strain ACM941 and other strains to various fungal toxins has long been attributed to membrane transporters, largely based on the relatively high number of ABC-transporter genes in their genome and/or their increased transcriptional activity upon exposure to toxigenic fungi. Notably, *C. rosea* ABC transporter genes are reported to be upregulated upon exposure to fungal mycotoxins (such as the *Fusarium* mycotoxin ZEA), bacterial toxins from *Pseudomonas chlororaphis*, or fungicides like Boscalid (Kamou et al. 2016). However, the exact role and the extent to which ABC transporters contribute to toxin tolerance has yet to be elucidated. For example, the yeast ABC transporter *pdr5* is upregulated upon exposure to DON and its deletion or mutation of key residues in its active site reduced tolerance for DON *in vivo*

(Gunter et al. 2016). However, pdr5's role in direct transport of DON has not been established. Similarly, despite *C. rosea* strain IK726 *pdr5* transcriptional activity and deletion assay results (Dubey et al. 2014; Kosawang et al. 2014), ZEA is detoxified by ZHD101 enzyme (Takahashi-Ando et al. 2002). In agreement with these reports, exometabolomic analysis established that 15-ADON was transformed to 15-ADON-3-Glc accumulating in the agar proximal to *C. rosea*, suggesting a role for enzymatic detoxification and possibly membrane transport in the tolerance process. The detoxification of 15-ADON in *C. rosea* is achieved (wholly, or at least in part) through glycosylation, possibly mediated by a glycosyltransferase enzyme, and is likely exported by a membrane transport system composed of either MFSs or ABC transporters. In support of this hypothesis, two ABC transporter homologs and several MFSs with homology to those implicated in xenobiotic tolerance were upregulated in *C. rosea* (Table 4). That said, the possibility that the detoxifying enzyme is itself secreted, eliminating the need for small molecular transport, cannot be strictly eliminated at this time.

Glycosylation of DON by partially resistant plants (Li et al. 2015, 2017; Steiner et al. 2017), and *Trichoderma spp* has been reported previously (Tian et al. 2016a, b, 2018). However, this is the first report involving direct glycosylation of 15-ADON. Notably, a recent report concluded that *C. rosea* stimulates the ability of maize to elicit the glycosylation of DON (Abdallah et al. 2018). However, this current study now provides substantial evidence that *C. rosea* is itself capable of 15-ADON glycosylation, and thus the possibility that *C. rosea* may have contributed to the glycosylation reaction reported for maize plants challenged with *F. graminearum* and *C. rosea* must be considered (Abdallah et al. 2018).

MFSs are the most common upregulated genes reported in several fungal-fungal interaction studies. In this study, 43 of the 67 (63 + 4 duplicates) differentially regulated *C. rosea*

MFSs were upregulated AC with *F. graminearum* mycelia. Interestingly, these MFSs were mainly dominated by those classified under sugar transporters family (2.A.1.1) and the anion:cation symporter (ACS) family (2.A.1.14), with 15 and 12 members each, respectively. Representation in the symporter family was largely dominated by the high affinity nicotinate permeases (2.A.1.14.11), while the galacturonic acid uptake porter (2.A.1.1.119) dominated the sugar transporter family. In general, sugar transporters and ACS family MFS encoding genes are enriched in endophytic microbe genomes because they are involved in nutrient acquisition from their host. For example, *Pestalotiopsis fici* (a pathogenic plant endophyte) had four times more ACS family genes compared to other studied genomes (Wang et al. 2015). Notably, the expression profile of these transcripts correlated well with the upregulation of cell wall degradative enzyme encoding transcripts. In contrast, MFSs family 2.A.1.3 (xenobiotic secretion) expression profile correlates well with the upregulation of secondary metabolism related gene clusters, as described above. Taken together, these results emphasize that the *C. rosea* transcriptomic response profile transitions from one dominated by secondary metabolism during the BC stage, to cell wall degradation and nutrient acquisition AC, in its confrontation with *F. graminearum*. Fungal lifestyle transitions depending on available nutrient source is a well-established phenomenon. Indeed the lifestyle of *Colletotrichum* (a plant pathogen) transitions from secondary metabolism biosynthesis during colonization to cell wall degradative enzyme encoding genes at the necrotrophic stage (Gan et al. 2013; O'Connell et al. 2012).

Finally, the observed *C. rosea* transition from secondary metabolism BC to necrotrophism AC with *F. graminearum*, was also accompanied by upregulation of gene clusters likely to play a role in expansion of its carbon source utilization. One such example is the up regulation of the ethanol utilization pathway (Flipphi et al. 2003). This pathway was first

described in *Aspergillus nidulans* where its expression enabled the fungus to utilize a wide range of organic compounds as sole sources of carbon and nitrogen. Upregulation of the putative alcS gene cluster in *C. rosea* occurred upon contact with *F. graminearum* and/or coincided with *C. rosea* moving to a resource depleted area of the agar plate (Table **S7**), heightens the plausibility that *C. rosea* expresses the alcS pathway to catabolize an alternative carbon source.

In conclusion, the results highlighted here demonstrate that the antagonistic response of the *C. rosea* (strain AMC941) towards *F. graminearum* (strain GZ3639) is initiated before the two organisms come into direct contact, and includes upregulation of secondary metabolism related genes and metabolite production. While trichothecenes are the main defense arsenal produced by *F. graminearum*, *C. rosea* produces a multitude of different metabolites mainly representing polyketides - trichodimerol and related analogs of TMC-151. The abundance of secondary metabolism related transcripts returns to basal level while *C. rosea* transitions to activating the transcription of genes encoding cell wall degradation enzymes upon actual contact with *F. graminearum*. The majority of cell wall degradation related transcripts weren't differentially regulated at BC. Notably, findings herein also demonstrate that one method of *C. rosea* tolerance of *F. graminearum* trichothecenes is via glycosylation to 15-ADON-3-Glc. While efforts are ongoing to identify the mechanistic components underlying this, it must be emphasized that this is the first report to describe a trichothecene detoxification functionality for *C. rosea*. Overall, a number of signature molecular mechanisms responsible for *C. rosea*'s antagonistic activity against *F. graminearum,* as well as its mycotoxin tolerance, were identified in this study, yielding several new testable hypotheses toward understanding the basis of naturally occurring biocontrol with potential applications for agronomic development in the future.

MATERIALS AND METHODS

Fungal strains and culture condition

C. rosea strain ACM941 (American Type Culture Collection ATCC 74447), provided by Dr. Allen Xue (Ottawa Research and Development Centre, AAFC) with permission from Adjuvant Plus Inc. (Kingsville, Canada), was grown at 25 °C for 10 – 12 days and maintained on potato dextrose broth (Bioshop, Canada) containing 15 g l^{-1} bacto agar (Difco laboratories, USA) (PDA) plates at 4 °C for short term storage. *F. graminearum* strain GZ3639 (Proctor et al. 1995), obtained from Dr. Susan McCormick (USDA, Peoria, IL), was grown for 5 – 6 days and was maintained as per *C. rosea*. For long term storage, agar plugs (5 – 6) taken from the growing edge of each fungal colony were used to inoculate carboxymethylcellulase (CMC) media (NH_4NO_3: 1 g l^{-1}; KH_2PO_4: 1 g l^{-1}; $MgSO_4$. $7H_2O$: 0.5 g l^{-1}; Yeast Extract: 1.0 g $l^{-1}$and CMC: 15 g l^{-1}) and grown for 10 days at 25 °C. Following mycelial removal by filtering the media through 4 – 5 layers of cheesecloth, macroconidia were pelleted by centrifugation at 4,000 × g for 20 min at 4 °C and washed twice using sterile-water. Macroconidia were re-suspended in 0.5 – 1 ml sterile-water and the concentration determined by counting using a hemocytometer. The final concentration of macroconidia in this stock was adjusted to 10^7 ml^{-1} in sterile-water containing 20% glycerol, flash-frozen in liquid nitrogen and stored at -80 °C. The 15-ADON standard was purchased from Cayman Chemical (Ann Arbor, MI), the ZEA standard was purchased from Sigma (Canada), and the gramillin standard was obtained from Barbara Blackwell.

An agar plug of the actively growing edge of *C. rosea* mycelia (harvested using the wide-end of a 1 ml sterile pipette tip for consistency) was inoculated on PDA plates ~1 cm away from the edge of the plate and grown in the dark at 25-28 °C. After growing *C. rosea* for ten days

alone (or after the mycelium covered approximately one third of the plate), agar plug of actively growing *F. graminearum* edge was inoculated (~1 cm away from the side of the plate) on the opposite side of the plate from where *C. rosea* was inoculated. Controls for each strain were inoculated similarly, but grown as mono-cultures. Early inoculation of *C. rosea* was necessary to compensate for the slow growing nature of the fungus, allowing for sufficient mycelia to accumulate for RNA extraction (see below). The experiment was set-up as a 7 day time course (post inoculation of *F. graminearum*). For metabolomics analyses, sampling occurred on days 3, 4, 5, and 7, where six agar plugs were excised using a core borer from the agar adjacent to the colony periphery (of both *C. rosea* and *F. graminearum* colonies) and stored in scintillation vials at -80 ℃ until metabolites were extracted. The experiment was done in six replicates, with individual plates for each of the different sampling time points. For transcriptomic analyses, samples were collected first, when the growing edges of *C. rosea* and *F. graminearum* in confrontation plates were ~ 1 cm apart (day 5), referred to as "before contact" (BC), and second, 12 - 16 hours after the growing edges of *C. rosea* and *F. graminearum* colonies in confrontation plates made contact (with no visible gap in between; day 7), referred to as "after contact" (AC) (Fig. S1). *C. rosea* and *F. graminearum* colony mycelia were scraped from both control and co-culture plates for RNA extraction, following the excision of the agar plugs for metabolomics analysis as described above (Fig. S1). Mycelia were flash frozen in liquid nitrogen and used for total RNA isolation either immediately or after a brief storage in a -80℃ freezer.

Secreted secondary metabolite profiling and metabolomic analysis

Each sample was extracted with 10 ml of ethyl acetate for 1.5 h, gently shaking at 150 rpm and the resulting extracts were evaporated to dryness. Extracts were subsequently reconstituted in MeOH to a concentration of 500 µg ml^{-1} and chemically profiled in a randomized order using

a Thermo Ultimate 3000 ultra-high performance liquid chromatography (UPLC) coupled to a Thermo LTQ Orbitrap XL high resolution mass spectrometer (HRMS). Chromatography was performed on a Phenomenex C_{18} Kinetex column (50 mm x 2.1 mm ID, 1.7 µm) with a flow rate of 0.35 ml min^{-1}, running a gradient of H_2O (+ 0.1 % formic acid) and ACN (+ 0.1 % formic acid): starting at 5 % ACN increasing to 95 % ACN by 4.5 mins and held at 95 % ACN until 8.0 mins until returning to 5 % ACN by 9 mins and holding to allow the column to equilibrate to starting conditions by 10 mins. The HRMS was operated in ESI^+ mode (with a *m/z* 100-2000 m/z range) using the following parameters: sheath gas (40), auxiliary gas (5), sweep gas (2), spray voltage (4.2 kV), capillary temperature (320 ˚C), capillary voltage (35 V), and tube lens (100 V).

All ".RAW" data files including samples, MeOH blanks (run after every sixth sample), and medium controls, were processed using MZMine v2.29 (Cell Unit, Okinawa Institute of Science and Technology [OIST], Onna, Okinawa, Japan). For data preprocessing, mass detection was carried out with a noise cut-off level of (5.0 E^5) using the FWHM (Full Width at Half Maximum) algorithm and deconvoluted with a chromatographic threshold of 35 %, a RT range minimum of 0.05 min, a minimum relative height of 35.0 %, and a minimum ratio of peak top/edge of 1.2. Data was then cleared of isotopes, aligned, and converted into a data matrix of discriminate variables (based on retention time (RT) and mass to charge ratio (*m/z*)) based on peak area measurements. Peaks were aligned using the Join Alignment function (with a *m/z* tolerance of 5.0 ppm and a RT tolerance of 0.1 min with a 20:10 weight for *m/z* vs. RT). Gaps in the data set where variables fell below the noise limit detection threshold were backfilled using a gap-filling algorithm (using a *m/z* tolerance of 5 ppm and RT tolerance of 0.05 min). Peak area values were normalized by dividing by the total ion current for each sample. Multivariate and univariate

statistical analysis was performed in the R environment using the "muma" package and Metaboanalyst.

A database of secondary metabolites previously reported from *C. rosea* and *F. graminearum* was compiled from a comprehensive literature search to generate a mass list of expected pseudomolecular ions (protonated mass, adducts, neutral losses, fragments) and used for signal annotation. For confirmation of signal annotations, in-source fragmentation and MS/MS experiments were carried out along with comparison of UV-absorbance spectra to literature values, and when possible, compared to standards (ie. 15-ADON and other associated trichothecenes, gramillins, culmorin, and zearalanone).

Confirmation of 15-ADON glycosylation by *C. rosea*.

To confirm 15-ADON glycosylation ability, *C. rosea* was grown on PDA plates for ten days and triplicate sterile filter discs (dosed with 50 µl of differing concentrations of 15-ADON (125 µg ml^{-1}, 250 µg ml^{-1} or 500 µg ml^{-1}) or MeOH vehicle control) were placed ~1.5 cm away from the fungal edge. After 6 days of incubation, the agar on either side of the filter discs was excised, extracted in ethyl acetate for 2 hrs, dried down and reconstituted in 1 ml of MeOH for UPLC-HRMS analysis. The experiment was performed in triplicate.

Transcriptome profiling

Total RNA extraction and RNA-Seq Freeze-dried mycelium (both *C. rosea* and *F. graminearum*) was ground to a fine powder and homogenized in 1 ml TRIzol® reagent (Thermo Fisher Scientific). The InviTrap® Spin Universal RNA Mini Kit (Stratec molecular, Germany) was used to purify total RNA (free of genomic DNA) from TRIzol aqueous phase, as per the manufacturer's protocol; the RNA concentration and purity was subsequently determined using a

Nanodrop spectrophotometer ND-1000 (Thermo Scientific). RNAseq libraries were prepared using TruSeq Stranded RNALT kit, and sequenced on an Illumina HiSeq 2500 platform according to the manufacturer's guidelines (Illumina, USA).

Differential gene expression analysis and validation

C. rosea: Trimmomatic software v0.36.4 (http://www.usadellab.org/cms/index.php?page=trimmomatic) was used to trim low quality short reads, and adapter and other Illumina-specific sequences with the following modifications to the default settings: leading low quality cutoff was 17; sliding window was 5 bp with a minimum average quality score of 20, and read length cutoff was 60 bp instead of 36 bp (Bolger et al. 2014). Paired-end *C. rosea* strain ACM941 reads were cleaned and mapped to *C. rosea* strain IK726 putative transcripts (accessed on Sept 14, 2017) using the read mapper software STAR version 2.5.1 b (Dobin et al. 2013). Raw read counts per gene were extracted with the software HTSeq-count v0.6.0 (Anders et al. 2015) following procedures described previously (Pertea et al. 2016, 2015). The DESeq2 based SARTools (v1.5.1) pipeline was adopted for differential analysis of mapped *C. rosea* strain ACM941 RNAseq count data – co-culture relative to monoculture (Varet et al. 2016). A BH *p*-value adjustment was performed (Benjamini and Hochberg 1995; Benjamini and Yekutieli 2001) and the false discovery rate (FDR) was set at $p < 0.05$. For comparison, high quality *C. rosea* strain ACM941 reads were mapped against *C. rosea* strain CBS12511 genome and annotated genes (unpublished data made available by JGI) as described above. Coding sequences (CDS) of each gene were subtracted from the reference genome sequence with the following tools: bedopts v2.4.19 (Neph et al. 2012) and bedtools v2.26.0 (Quinlan and Hall 2010), and raw read counts per gene extraction and subsequent differential gene expression analysis was performed as described above. Blastx-fast (*E*-value <

10^{-3}) module of BLAST2Go was used to align translated *C. rosea* transcripts (upregulated >2.5 fold BC and AC) against the NR database (NCBI non-redundant protein library—last accessed April 20, 2019) to improve annotation coverage. After annotation, gene ontology (GO) terms and enzyme codes associated with each transcript were retrieved using default parameters to determine their biological role and for graphical presentations.

To validate RNAseq gene expression results, primers (Table S2) were designed using the IDT primer quest software (https://www.idtdna.com/Primerquest/Home/Index) targeting 190–200 base-pairs (bp) fragments. cDNA was synthesized from total RNA stored at −80 °C (remaining from samples shipped for sequencing) using the 5X All-In-One RT MasterMix Kit (ABM, Inc., Canada). The relative transcript abundance of the selected genes was assessed by IQ™5 multicolor real-time PCR detection system (Bio-Rad, USA) using the EvaGreen Express 2X qPCR MasterMix (ABM, Inc., Canada) along with approximately 150 ng of cDNA template and 500 nM of each of the primers in a 20 µl reaction volume. The following program was used for RT-qPCR: 95 °C for 1 min followed by 40 cycles of 5 s at 95 °C and 15 s at 59°C. Normalized relative expression values ($\Delta\Delta C_T$) of the selected candidates were calculated using the formula $2^{-\Delta\Delta CT}$ (Livak and Schmittgen 2001), using *EF1α* and *β-actin* as reference genes (Table S2). Serial dilutions of cDNA samples were used to develop standard curves for primer sets to confirm their efficiency according to the Livak relative-gene expression quantification method.

F. graminearum: The *F. graminearum* RNA-Seq data was analyzed using CLC Genomics workbench version 11.0.1 (Qiagen Corp.). Raw data was trimmed based on default quality scores that were determined by the base caller error probability level ($P < 0.01$). To estimate the expression levels, high quality RNA sequences were aligned to the *F. graminearum* RR1.36

genome annotated with genes and transcripts (King et al. 2015) (ftp://ftp.ensemblgenomes.org/pub/fungi/release-36/fasta/fusarium_graminearum/). Read alignment was performed using high stringency criteria to eliminate *C. rosea* transcripts: similarity fraction = 0.95 and length fraction = 0.8, mismatch cost = 2, deletion and insertion costs = 3 and maximum number of hits per read = 10. Gene expression levels were estimated as transcripts per million (TPM) (Li et al. 2010) which was calculated as: $TPM = (RPKM \times 10^6) / \Sigma RPKM$, where the sum is over the *RPKM* values of all genes/transcripts. Reads per kilobase of exon model per million mapped reads (RPKM) (Mortazavi et al. 2008) was calculated following the formula: RPKM = total exon reads / [mapped reads (millions) × exon length (KB)].

An empirical analysis of differential gene expression or the 'exact test' according to (Robinson and Smyth 2008) was implemented to compare mono-cultured versus co-cultured fungal inoculations. The 'exact test', a package also incorporated in EdgeR Bioconductor (Robinson et al. 2010), is similar to Fisher's exact test but also accounts for over dispersion caused by biological variability. Transcripts were considered as significantly differentially expressed when fold change was ≥ 4.0, False Discovery Rate (FDR) (Benjamini and Hochberg 1995) corrected $P \leq 0.005$ among groups in at least one of the groups compared. Gene annotation and GO enrichment analysis for *F. graminearum* was accomplished within the FungiDB database (https://fungidb.org/fungidb/) (Basenko et al. 2018; Stajich et al. 2012).

To validate the RNAseq gene expression results, cDNA was synthesized using total RNA with the iScript Reverse Transcription Supermix for RT-qPCR (Bio-Rad Laboratories Canada Ltd.) as described by the manufacturer. 4 µl of a 50-fold dilution (BC) or of a 20-fold dilution (AC) of the cDNA was used in each 20 µl Droplet Digital PCR (ddPCR) reaction along with 10 µl 2X QX200 ddPCR EvaGreen Supermix, 200nM of each primer and DNAse-free water.

Primers were designed to differentiate between genomic DNA and cDNA for most genes (Table S2). A no-template control was added for each primer pair. Droplets were generated as per manufacturer's instructions (Bio-Rad Laboratories Canada Ltd.) and transferred to a TwinTec 96-well PCRS45 plate (Eppendorf Canada Ltd.) and cycled on a C1000 Touch Thermal Cycler (Bio-Rad Laboratories Canada Ltd.) using the default EvaGreen Supermix amplification protocol at an annealing temperature of 58 °C for each primer pair. Optimal annealing temperature was determined by running a temperature gradient for each primer pair ranging from 55 °C to 61 °C. Following amplification, the reaction plate was loaded on the QX200 Droplet Reader for detection. Data was analyzed using the instrument software, QuantaSoft version 1.6.6.0320 (Bio-Rad Laboratories Canada Ltd.), and imported into Microsoft Excel for further analysis and normalization. Expression was normalized with two reference genes, *F. graminearum EF1α*, and *ßTUB* (Table S2).

Differentially regulated gene cluster mining

C. rosea strain IK726 transcript identifiers were consecutively numbered according to their relative locations on its genomic sequence (Karlsson et al. 2015). Since secondary metabolite biosynthesis-related genes are typically organized into gene clusters, we took advantage of the assigned transcript identifiers to manually screen the relative expression of transcripts surrounding upregulated secondary metabolite anchor genes – membrane transporter proteins, polyketide or non-ribosomal peptide synthases. If three or more consecutive transcripts surrounding a putative secondary metabolite gene were upregulated, their sequences were retrieved and blasted against IK726 genome and *C. rosea* strain CBS125111 to confirm their relative position. Putative cluster products were searched against the FungiSMASH online secondary metabolite prediction tool for verification and prediction (Medema et al. 2011). Up or

downregulated *F. graminearum* gene cluster analysis was based on predicted *F. graminearum* gene clusters (Sieber et al. 2014).

Statistical Analysis

All experiments were replicated at least three times, and one-way ANOVA and multiple mean separation modules of the GraphPad prism (version 7.0, Graphpad Software, San Diego, CA) were used to calculate statistical differences and compare the means, respectively.

ACKNOWLEDGEMENTS: We are grateful to Dr. Allen Xue (Agriculture and Agri-Food Canada, Ottawa, ON, Canada) and Dr. William G. Brown (Adjuvant Plus Inc., Kingsville, Canada) for providing *C. rosea* strain ACM941, Dr. Susan McCormick (USDA, Peoria, IL) for providing *F. graminearum* strain GZ3639 and Dr. Barbara Blackwell (AAFC, Ottawa, ON) for providing gramillin standard and 15-ADON. We thank Joey Spatafora and Kathryn Bushley for providing access to the unpublished *Clonostachys rosea* genome data of produced by the U.S. Department of Energy Joint Genome Institute, a DOE Office of Science User Facility, supported by the Office of Science of the U.S. Department of Energy under Contract No. DE-AC02-05CH11231. We also would like to thank Prof. Magnus Karlsson (SLU) for sharing *C. rosea strain* IK726 genomic and putative transcript libraries. This manuscript represents NRCC communication # 56458.

AUTHOR CONTRIBUTIONS: ZAD, TW, LJH, DPO and MCL contributed to design of the research, data analysis, interpretation and writing the manuscript. ZAD, TW, KAR, AS and AJ contributed to performance of the research, data collection and some interpretation. SJF contributed to data analysis.

REFERENCES:

Abdallah, M., De Boevre, M., Landschoot, S., De Saeger, S., Haesaert, G., and Audenaert, K. 2018. Fungal Endophytes Control *Fusarium graminearum* and Reduce Trichothecenes and Zearalenone in Maize. Toxins (Basel). 10 (12): 493. doi:10.3390/toxinS10120493

Almaguer, C., Mantella, D., Perez, E., and Patton-Vogt, J. 2003. Inositol and Phosphate Regulate GIT1 Transcription and Glycerophosphoinositol Incorporation *in Saccharomyces cerevisiae*. Eukaryotic Cell. 2:729–736

Anders, S., Pyl, P. T., and Huber, W. 2015. HTSeq—a Python framework to work with high-throughput sequencing data. Bioinformatics. 31:166–169

Atanasova, L., Dubey, M., Grujić, M., Gudmundsson, M., Lorenz, C., Sandgren, M., Kubicek, C. P., Jensen, D. F., and Karlsson, M. 2018. Evolution and functional characterization of pectate lyase PEL12, a member of a highly expanded *Clonostachys rosea* polysaccharide lyase 1 family. BMC Microbiology. 18:178

Atanasova-Penichon, V., Legoahec, L., Bernillon, S., Deborde, C., Maucourt, M., Verdal-Bonnin, M.-N., Pinson-Gadais, L., Ponts, N., Moing, A., and Richard-Forget, F. 2018. Mycotoxin Biosynthesis and Central Metabolism Are Two Interlinked Pathways in *Fusarium graminearum*, as Demonstrated by the Extensive Metabolic Changes Induced by Caffeic Acid Exposure. Appl. Environ. Microbiol. 84:e01705-17

Bahadoor, A., Brauer, E. K., Bosnich, W., Schneiderman, D., Johnston, A., Aubin, Y., Blackwell, B., Melanson, J. E., and Harris, L. J. 2018. Gramillin A and B: Cyclic Lipopeptides Identified as the Nonribosomal Biosynthetic Products of *Fusarium graminearum*. J. Am. Chem. Soc. 140:16783–16791

Basenko, E. Y., Pulman, J. A., Shanmugasundram, A., Harb, O. S., Crouch, K., Starns, D., Warrenfeltz, S., Aurrecoechea, C., Stoeckert, C. J., Kissinger, J. C., Roos, D. S., and Hertz-Fowler, C. 2018. FungiDB: An Integrated Bioinformatic Resource for Fungi and Oomycetes. J Fungi (Basel). 4 (1). pii: E39. doi: 10.3390/jof4010039.

Benjamini, Y., and Hochberg, Y. 1995. Controlling the False Discovery Rate: A Practical and Powerful Approach to Multiple Testing. Journal of the Royal Statistical Society. Series B (Methodological). 57:289–300

Benjamini, Y., and Yekutieli, D. 2001. The Control of the False Discovery Rate in Multiple Testing under Dependency. The Annals of Statistics. 29:1165–1188

Bolger, A. M., Lohse, M., and Usadel, B. 2014. Trimmomatic: a flexible trimmer for Illumina sequence data. Bioinformatics. 30:2114–2120

Brady, P. S., Scofield, R. F., Schumann, W. C., Ohgaku, S., Kumaran, K., Margolis, J. M., and Landau, B. R. 1982. The tracing of the pathway of mevalonate's metabolism to other than sterols. J. Biol. Chem. 257:10742–10746

Chatterjee, S., Kuang, Y., Splivallo, R., Chatterjee, P., and Karlovsky, P. 2016. Interactions among filamentous fungi *Aspergillus niger*, *Fusarium verticillioides* and *Clonostachys rosea*: fungal biomass, diversity of secreted metabolites and fumonisin production. BMC Microbiology. 16:83 DOI 10.1186/S12866-016-0698-3.

Demissie, Z. A., Foote, S. J., Tan, Y., and Loewen, M. C. 2018. Profiling of the transcriptomic responses of *Clonostachys rosea* upon treatment with *Fusarium graminearum* secretome. Frontiers in microbiology. 9:1061. doi: 10.3389/fmicb.2018.01061.

Dobin, A., Davis, C. A., Schlesinger, F., Drenkow, J., Zaleski, C., Jha, S., Batut, P., Chaisson, M., and Gingeras, T. R. 2013. STAR: ultrafast universal RNA-seq aligner. Bioinformatics. 29:15–21

Dubey, M. K., Jensen, D. F., and Karlsson, M. 2014. An ATP-Binding Cassette Pleiotropic Drug Transporter Protein Is Required for Xenobiotic Tolerance and Antagonism in the Fungal Biocontrol Agent *Clonostachys rosea*. MPMI. 27:725–732

Evidente, A., Andolfi, A., Cimmino, A., Ganassi, S., Altomare, C., Favilla, M., De, A. C., Vitagliano, S., and Agnese, M. S. 2009. Bisorbicillinoids produced by the fungus *Trichoderma citrinoviride* affect feeding preference of the aphid *Schizaphis graminum*. J Chem Ecol. 35:533–541

Flipphi, M., Kocialkowska, J., and Felenbok, B. 2003. Relationships between the ethanol utilization (alc) pathway and unrelated catabolic pathways in *Aspergillus nidulans*. European Journal of Biochemistry. 270:3555–3564

Flipphi, M., Robellet, X., Dequier, E., Leschelle, X., Felenbok, B., and Vélot, C. 2006. Functional analysis of alcS, a gene of the alc cluster in *Aspergillus nidulans*. Fungal Genetics and Biology. 43:247–260

Frandsen, R. J. N., Schutt, C., Lund, B.W., Staerk, D., Nielsen, J., Olsson, S. 2011. Two novel classes of enzymes are required for the biosynthesis of aurofusarin in *Fusarium graminearum*. The Journal of Biological Chemistry 286: 10419-10428.

Gan, P., Ikeda, K., Irieda, H., Narusaka, M., O'Connell, R. J., Narusaka, Y., Takano, Y., Kubo, Y., and Shirasu, K. 2013. Comparative genomic and transcriptomic analyses reveal the hemibiotrophic stage shift of *Colletotrichum* fungi. New Phytologist. 197:1236–1249

Gbelska, Y., Krijger, J.-J., and Breunig, K. D. 2006. Evolution of gene families: the multidrug resistance transporter genes in five related yeast species. FEMS Yeast Res. 6:345–355

Gunter, A. B., Hermans, A., Bosnich, W., Johnson, D. A., Harris, L. J., and Gleddie, S. 2016. Protein engineering of *Saccharomyces cerevisiae* transporter Pdr5p identifies key residues that impact *Fusarium* mycotoxin export and resistance to inhibition. MicrobiologyOpen. 5:979–991

Guzmán‐Chávez, F., Salo, O., Nygård, Y., Lankhorst, P. P., Bovenberg, R. A. L., and Driessen, A. J. M. 2017. Mechanism and regulation of sorbicillin biosynthesis by *Penicillium chrysogenum*. Microb Biotechnol. 10:958–968

Hue, A. G., Voldeng, H. D., Savard, M. E., Fedak, G., Tian, X., and Hsiang, T. 2009. Biological control of fusarium head blight of wheat with *Clonostachys rosea* strain ACM941. Canadian Journal of Plant Pathology. 31:169–179

Iqbal, M., Dubey, M., Broberg, A., Viketoft, M., Funck Jensen, D., and Karlsson, M. 2019. Deletion of the Non-Ribosomal Peptide Synthetase Gene npS1 in the Fungus *Clonostachys rosea* Attenuates Antagonism and Biocontrol of Plant Pathogenic *Fusarium* and Nematodes. Phytopathology. DOI: 10.1094/PHYTO-02-19-0042-R.

Jin, J.M., Lee, .J, Lee, Y.W. 2010. Characterization of carotenoid biosynthetic genes in the *ascomycete Gibberella zeae*. FEMS microbiology letters. 302:197-202.

Ju, Y. M., Juang, S. H., Chen, K. J., and Li, Z.-H. 2007. TMC-151 a monoacetate, a new polyketide from Bionectria ochroleuca. zeitschrift fur naturforschung - section b journal of chemical sciences. 62:561–564

Kamou, N. N., Dubey, M., Tzelepis, G., Menexes, G., Papadakis, E. N., Karlsson, M., Lagopodi, A. L., and Jensen, D. F. 2016. Investigating the compatibility of the biocontrol agent

Clonostachys rosea IK726 with prodigiosin-producing *Serratia rubidaea* S45 and phenazine-producing *Pseudomonas chlororaphis* ToZa7. Arch. Microbiol. 198:369–377

Karlsson, M., Atanasova, L., Jensen, D. F., and Zeilinger, S. 2017. Necrotrophic Mycoparasites and Their Genomes. Microbiology Spectrum. 5(2):FUNK-0016-2016. doi:10.1128/microbiolspec.FUNK-0016-2016.

Karlsson, M., Durling, M. B., Choi, J., Kosawang, C., Lackner, G., Tzelepis, G. D., Nygren, K., Dubey, M. K., Kamou, N., Levasseur, A., Zapparata, A., Wang, J., Amby, D. B., Jensen, B., Sarrocco, S., Panteris, E., Lagopodi, A. L., Pöggeler, S., Vannacci, G., Collinge, D. B., Hoffmeister, D., Henrissat, B., Lee, Y.-H., and Jensen, D. F. 2015. Insights on the Evolution of Mycoparasitism from the Genome of *Clonostachys rosea*. Genome Biol Evol. 7:465–480

Keller, N. P. 2019. Fungal secondary metabolism: regulation, function and drug discovery. Nature Reviews Microbiology. 17:167–180

King, R., Urban, M., Hammond-Kosack, M. C. U., Hassani-Pak, K., and Hammond-Kosack, K. E. 2015. The completed genome sequence of the pathogenic ascomycete fungus *Fusarium graminearum*. BMC Genomics. 16:544 DOI 10.1186/S12864-015-1756-1.

Kohno, J., Nishio, M., Sakurai, M., Kawano, K., Hiramatsu, H., Kameda, N., Kishi, N., Yamashita, T., Okuda, T., and Komatsubara, S. 1999. Isolation and structure determination of TMC-151s: Novel polyketide antibiotics from *Gliocladium catenulatum* Gilman & Abbott TC 1280. Tetrahedron. 55:7771–7786

Kosawang, C., Karlsson, M., Jensen, D. F., Dilokpimol, A., and Collinge, D. B. 2014. Transcriptomic profiling to identify genes involved in *Fusarium* mycotoxin

Deoxynivalenol and Zearalenone tolerance in the mycoparasitic fungus *Clonostachys rosea*. BMC Genomics. 15:55

Lenburg, M. E., and O'Shea, E. K. 1996. Signaling phosphate starvation. Trends in Biochemical Sciences. 21:383–387

Li, B., Ruotti, V., Stewart, R. M., Thomson, J. A., and Dewey, C. N. 2010. RNA-Seq gene expression estimation with read mapping uncertainty. Bioinformatics. 26:493–500

Li, G., Huang, H., Kokko, E., and Acharya, S. 2002. Ultrastructural study of mycoparasitism of *Gliocladium roseum* on *Botrytis cinerea*. Bot. Bull. Acad. Sin. 43:211–218

Li, X., Michlmayr, H., Schweiger, W., Malachova, A., Shin, S., Huang, Y., Dong, Y., Wiesenberger, G., McCormick, S., Lemmens, M., Fruhmann, P., Hametner, C., Berthiller, F., Adam, G., and Muehlbauer, G. J. 2017. A barley UDP-glucosyltransferase inactivates nivalenol and provides Fusarium Head Blight resistance in transgenic wheat. J Exp Bot. 68:2187–2197

Li, X., Shin, S., Heinen, S., Dill-Macky, R., Berthiller, F., Nersesian, N., Clemente, T., McCormick, S., and Muehlbauer, G. J. 2015. Transgenic wheat expressing a barley UDP-glucosyltransferase detoxifies deoxynivalenol and provides high levels of resistance to *Fusarium graminearum*. Molecular Plant-Microbe Interactions. 28:1237–1246

Livak, K. J., and Schmittgen, T. D. 2001. Analysis of Relative Gene Expression Data Using Real-Time Quantitative PCR and the $2^{-\Delta\Delta CT}$ Method. Methods. 25:402–408

Luo, Z., Ren, H., Mousa, J. J., Rangel, D. E. N., Zhang, Y., Bruner, S. D., and Keyhani, N. O. 2017. The PacC transcription factor regulates secondary metabolite production and stress response, but has only minor effects on virulence in the insect pathogenic fungus *Beauveria bassiana*. Environmental Microbiology. 19:788–802

Lysøe, E., Dees, M. W., and Brurberg, M. B. 2017. A Three-Way Transcriptomic Interaction Study of a Biocontrol Agent (*Clonostachys rosea*), a Fungal Pathogen (*Helminthosporium solani*), and a Potato Host (*Solanum tuberosum*). MPMI. 30:646–655

Medema, M. H., Blin, K., Cimermancic, P., de Jager, V., Zakrzewski, P., Fischbach, M. A., Weber, T., Takano, E., and Breitling, R. 2011. antiSMASH: rapid identification, annotation and analysis of secondary metabolite biosynthesis gene clusters in bacterial and fungal genome sequences. Nucleic Acids Res. 39:W339–W346

Medentsev AG, Kotik AN, Trufanova VA, Akimenko VK. 1993. Identification of aurofusarin in *Fusarium graminearum* isolates, causing a syndrome of worsening of egg quality in chickens. Prikladnaia biokhimiia i mikrobiologiia. 29: 542-546.

Mortazavi, A., Williams, B. A., McCue, K., Schaeffer, L., and Wold, B. 2008. Mapping and quantifying mammalian transcriptomes by RNA-Seq. Nature Methods. 5:621–628

Neph, S., Kuehn, M. S., Reynolds, A. P., Haugen, E., Thurman, R. E., Johnson, A. K., Rynes, E., Maurano, M. T., Vierstra, J., Thomas, S., Sandstrom, R., Humbert, R., and Stamatoyannopoulos, J. A. 2012. BEDOPS: high-performance genomic feature operations. Bioinformatics. 28:1919–1920

Niehaus, E.-M., Kleigrewe, K., Wiemann, P., Studt, L., Sieber, C. M. K., Connolly, L. R., Freitag, M., Güldener, U., Tudzynski, B., and Humpf, H.-U. 2013. Genetic Manipulation of the *Fusarium fujikuroi* Fusarin Gene Cluster Yields Insight into the Complex Regulation and Fusarin Biosynthetic Pathway. Chemistry & Biology. 20:1055–1066

Nygren, K., Dubey, M., Zapparata, A., Iqbal, M., Tzelepis, G. D., Durling, M. B., Jensen, D. F., and Karlsson, M. 2018. The mycoparasitic fungus *Clonostachys rosea* responds with both

common and specific gene expression during interspecific interactions with fungal prey. Evolutionary Applications. 11:931–949

O'Connell, R. J., Thon, M. R., Hacquard, S., Amyotte, S. G., Kleemann, J., Torres, M. F., Damm, U., Buiate, E. A., Epstein, L., Alkan, N., Altmüller, J., Alvarado-Balderrama, L., Bauser, C. A., Becker, C., Birren, B. W., Chen, Z., Choi, J., Crouch, J. A., Duvick, J. P., Farman, M. A., Gan, P., Heiman, D., Henrissat, B., Howard, R. J., Kabbage, M., Koch, C., Kracher, B., Kubo, Y., Law, A. D., Lebrun, M.-H., Lee, Y.-H., Miyara, I., Moore, N., Neumann, U., Nordström, K., Panaccione, D. G., Panstruga, R., Place, M., Proctor, R. H., Prusky, D., Rech, G., Reinhardt, R., Rollins, J. A., Rounsley, S., Schardl, C. L., Schwartz, D. C., Shenoy, N., Shirasu, K., Sikhakolli, U. R., Stüber, K., Sukno, S. A., Sweigard, J. A., Takano, Y., Takahara, H., Trail, F., van der Does, H. C., Voll, L. M., Will, I., Young, S., Zeng, Q., Zhang, J., Zhou, S., Dickman, M. B., Schulze-Lefert, P., Ver Loren van Themaat, E., Ma, L.-J., and Vaillancourt, L. J. 2012. Lifestyle transitions in plant pathogenic *Colletotrichum* fungi deciphered by genome and transcriptome analyses. Nature Genetics. 44:1060–1065

Oide, S., Berthiller, F., Wiesenberger, G., Adam, G., Turgeon, B.G. 2015. Individual and combined roles of malonichrome, ferricrocin, and TAFC siderophores in *Fusarium graminearum* pathogenic and sexual development. Frontiers in Microbiology 5: 579.

Okada, B. K., Seyedsayamdost, M. R., and Shen, A. 2017. Antibiotic dialogues: induction of silent biosynthetic gene clusters by exogenous small molecules. FEMS Microbiol Rev. 41:19–33

Okuda, T., Kohno, J., Kishi, N., Asai, Y., Nishio, M., and Komatsubara, S. 2000. Production of TMC-151, TMC-154 and TMC-171, a new class of antibiotics, is specific to '*Gliocladium roseum*' group. Mycoscience. 41:239–253

Pachenari, A., and Dix, N. J. 1980. Production of toxins and wall degrading enzymes by *Gliocladium roseum*. Transactions of the British Mycological Society. 74:561–566

Pertea, M., Kim, D., Pertea, G., Leek, J. T., and Salzberg, S. L. 2016. Transcript-level expression analysis of RNA-seq experiments with HISAT, StringTie, and Ballgown. Nature protocols. 11:1650

Pertea, M., Pertea, G. M., Antonescu, C. M., Chang, T.-C., Mendell, J. T., and Salzberg, S. L. 2015. StringTie enables improved reconstruction of a transcriptome from RNA-seq reads. Nat. Biotechnol. 33:290–295

Proctor, R. H., Hohn, T. M., and McCormick, S. P. 1995. Reduced virulence of *Gibberella zeae* caused by disruption of a trichothecene toxin biosynthetic gene. Mol. Plant Microbe Interact. 8:593–601

Quinlan, A. R., and Hall, I. M. 2010. BEDTools: a flexible suite of utilities for comparing genomic features. Bioinformatics. 26:841–842

Riekhof, W. R., Naik, S., Bertrand, H., Benning, C., and Voelker, D. R. 2014. Phosphate Starvation in Fungi Induces the Replacement of Phosphatidylcholine with the Phosphorus-Free Betaine Lipid Diacylglyceryl-N,N,N-Trimethylhomoserine. Eukaryotic Cell. 13:749–757

Robinson, M. D., McCarthy, D. J., and Smyth, G. K. 2010. edgeR: a Bioconductor package for differential expression analysis of digital gene expression data. Bioinformatics. 26:139–140

Robinson, M. D., and Smyth, G. K. 2008. Small-sample estimation of negative binomial dispersion, with applications to SAGE data. Biostatistics. 9:321–332

Rodríguez, J. M., Ruíz-Sala, P., Ugarte, M., and Peñalva, M. Á. 2004. Fungal Metabolic Model for 3-Methylcrotonyl-CoA Carboxylase Deficiency. J. Biol. Chem. 279:4578–4587

Rodríguez, M. a., Cabrera, G., Gozzo, F. c., Eberlin, M. n., and Godeas, A. 2011. *Clonostachys rosea* BAFC3874 as a *Sclerotinia sclerotiorum* antagonist: mechanisms involved and potential as a biocontrol agent. Journal of Applied Microbiology. 110:1177–1186

Saier, M. H., Reddy, V. S., Tsu, B. V., Ahmed, M. S., Li, C., and Moreno-Hagelsieb, G. 2016. The Transporter Classification Database (TCDB): recent advances. Nucleic Acids Res. 44:D372-379

Schmeitzl, C., Warth, B., Fruhmann, P., Michlmayr, H., Malachová, A., Berthiller, F., Schuhmacher, R., Krska, R., and Adam, G. 2015. The metabolic fate of deoxynivalenol and its acetylated derivatives in a wheat suspension culture: Identification and detection of DON-15-O-glucoside, 15-acetyl-DON-3-O-glucoside and 15-acetyl-DON-3-sulfate. Toxins. 7:3112–3126

Sieber, C. M. K., Lee, W., Wong, P., Münsterkötter, M., Mewes, H.-W., Schmeitzl, C., Varga, E., Berthiller, F., Adam, G., and Güldener, U. 2014. The *Fusarium graminearum* Genome Reveals More Secondary Metabolite Gene Clusters and Hints of Horizontal Gene Transfer. PLoS One. 9(10): e110311.

Sørensen, J. L., Hansen, F. T., Sondergaard, T. E., Staerk, D., Lee, T. V., Wimmer, R., Klitgaard, L. G., Purup, S., Giese, H., and Frandsen, R. J. N. 2012. Production of novel fusarielins by ectopic activation of the polyketide synthase 9 cluster in *Fusarium graminearum*. Environmental Microbiology. 14:1159–1170

Stajich, J. E., Harris, T., Brunk, B. P., Brestelli, J., Fischer, S., Harb, O. S., Kissinger, J. C., Li, W., Nayak, V., Pinney, D. F., Stoeckert, C. J., and Roos, D. S. 2012. FungiDB: an integrated functional genomics database for fungi. Nucleic Acids Res. 40:D675-681

Steiner, B., Buerstmayr, M., Michel, S., Schweiger, W., Lemmens, M., and Buerstmayr, H. 2017. Breeding strategies and advances in line selection for Fusarium head blight resistance in wheat. Trop. plant pathol. 42:165–174

Sun, Z.-B., Sun, M.-H., and Li, S.-D. 2015. Identification of mycoparasitism-related genes in *Clonostachys rosea* 67-1 active against *Sclerotinia sclerotiorum*. Scientific Reports. 5:srep18169

Sun, Z.-B., Sun, M.-H., Zhou, M., and Li, S.-D. 2017. Transformation of the endochitinase gene Chi67-1 in *Clonostachys rosea* 67-1 increases its biocontrol activity against *Sclerotinia sclerotiorum*. AMB Express. 7:1 DOI 10.1186/S13568-016-0313-x.

Sutton, J. C., Li, D.-W., Peng, G., Yu, H., Zhang, P., and Valdebenito-Sanhueza, R. M. 1997. *Gliocladium roseum* a versatile adversary of *Botrytis cinerea* in crops. Plant Disease. 81:316–328

Takahashi-Ando, N., Kimura, M., Kakeya, H., Osada, H., and Yamaguchi, I. 2002. A novel lactonohydrolase responsible for the detoxification of zearalenone: enzyme purification and gene cloning. Biochemical Journal. 365:1–6

Tian, Y., Tan, Y., Liu, N., Liao, Y., Sun, C., Wang, S., and Wu, A. 2016a. Functional Agents to Biologically Control Deoxynivalenol Contamination in Cereal Grains. Front. Microbiol. 7:395. doi: 10.3389/fmicb.2016.00395. eCollection 2016.

Tian, Y., Tan, Y., Liu, N., Yan, Z., Liao, Y., Chen, J., de Saeger, S., Yang, H., Zhang, Q., and Wu, A. 2016b. Detoxification of Deoxynivalenol via Glycosylation Represents Novel

Insights on Antagonistic Activities of *Trichoderma* when Confronted with *Fusarium graminearum*. Toxins (Basel). 8(11): 335. doi.org/10.3390/toxins8110335.

Tian, Y., Tan, Y., Yan, Z., Liao, Y., Chen, J., De Boevre, M., De Saeger, S., and Wu, A. 2018. Antagonistic and Detoxification Potentials of *Trichoderma* Isolates for Control of Zearalenone (ZEN) Producing *Fusarium graminearum*. Front. Microbiol. 8: 2710. doi: 10.3389/fmicb.2017.02710.

Utermark J, Karlovsky P. 2007. Role of zearalenone lactonase in protection of *Gliocladium roseum* from fungitoxic effects of the mycotoxin zearalenone. Appl. Environ. Microbiol.. 73: 637-42.

Varet, H., Brillet-Guéguen, L., Coppée, J.-Y., and Dillies, M.-A. 2016. SARTools: A DESeq2- and EdgeR-Based R Pipeline for Comprehensive Differential Analysis of RNA-Seq Data. PLOS ONE. 11:e0157022

Wang, X., Zhang, X., Liu, L., Xiang, M., Wang, W., Sun, X., Che, Y., Guo, L., Liu, G., Guo, L., Wang, C., Yin, W.-B., Stadler, M., Zhang, X., and Liu, X. 2015. Genomic and transcriptomic analysis of the endophytic fungus *Pestalotiopsis fici* reveals its lifestyle and high potential for synthesis of natural products. BMC Genomics. 16:28. doi: 10.1186/S12864-014-1190-9.

Xue, A. G. 2002. *Gliocladium roseum* strains useful for the control of fungal pathogens in plants. Patent number WO2000018241A1.

Xue, A. G., Chen, Y., Voldeng, H. D., Fedak, G., Savard, M. E., Längle, T., Zhang, J., and Harman, G. E. 2014. Concentration and cultivar effects on efficacy of CLO-1 biofungicide in controlling Fusarium head blight of wheat. Biological Control. 73:2–7

Yu, H., and Sutton, J. C. 1997. Morphological development and interactions of *Gliocladium roseum* and *Botrytis cinerea* in raspberry. Canadian Journal of Plant Pathology. 19:237–246

Zhai, M.-M., Qi, F.-M., Li, J., Jiang, C.-X., Hou, Y., Shi, Y.-P., Di, D.-L., Zhang, J.-W., and Wu, Q.-X. 2016. Isolation of Secondary Metabolites from the Soil-Derived Fungus *Clonostachys rosea* YRS-06, a Biological Control Agent, and Evaluation of Antibacterial Activity. Journal of Agricultural and Food Chemistry. 64:2298–2306

Zhang, L., Yang, J., Niu, Q., Zhao, X., Ye, F., Liang, L., and Zhang, K.-Q. 2008. Investigation on the infection mechanism of the fungus *Clonostachys rosea* against nematodes using the green fluorescent protein. Appl Microbiol Biotechnol. 78:983–990

Table 1. Expression of a putative *C. rosea* trichodimerol/bisorbicillinoid gene cluster detected by RNAseq. Fold change values in bold type are significant at p-value<0.05 while italicized fold change values are not (p-value >0.05).

Transcript ID	**Annotation**	**Before Contact** Fold Change (p-value)	**After Contact** Fold Change (p-value)
BN869_T00010687_1	sor8	**2.037 (9.52E-15)**	*1.784 (2.92E-52)*
BN869_T00010688_1	sor3	*1.567 (2.08E-07)*	*1.793 (9.57E-49)*
BN869_T00010689_1	sor6	**2.404 (2.51E-33**	*1.711 (1.33E-134)*
BN869_T00010690_1	esterase	*1.931 (1.64E-14)*	*1.854 (2.78E-60)*
BN869_T00010691_1	sor4	*0.923 (0.406422)*	*0.804 (5.58E-08)*
BN869_T00010692_1	sor5	**2.045 (7.97E-20)**	*1.036 (0.253954)*
BN869_T00010693_1	sor2	**2.165 (5.00E-18)**	*0.869 (0.013191)*
BN869_T00010694_1	sor1	**2.564 (3.44E-32**)	0.811 (9.03E-09)

Table 2. Expression of selected *C. rosea* cell wall degradation and proteolysis homeolog transcripts detected by RNAseq. Fold change values in bold type are significant at p-value<0.05 while italicized fold change values are not (p-value >0.05).

Transcript ID	Annotation	**Before Contact** Fold Change (p-value)	**After Contact** Fold Change (p-value)
Peptidase			
BN869_T00006507_1	fungalysin metallopeptidase	*1.7 (0.416)*	**3.5 (3.193E-15)**
Protease			
BN869_T00003885_1	metalloprotease	*0.2 (0.36)*	**16.5 (1.237E-38)**
BN869_T00011996_1	Trypsin-like serine protease	*1.2 (0.95)*	**6 (0.0063491)**
BN869_T00004333_1	metalloprotease	*1.3 (0.75)*	**5.1 (5.986E-39)**
BN869_T00008115_1	metalloprotease	*0.7 (0.08)*	**4 (1.387E-32)**
galacto/mano/sidase			
BN869_T00010437_1	beta-mannosidase	*1.2 (0.95)*	**22.1 (1.577E-06)**
BN869_T00012029_1	xylosidase arabinofuranosidase	*0.4 (0.314)*	**6.6 (0.0024205)**
BN869_T00010326_1	beta-galactosidase	**11.36 (0.015)**	*2.72 (0.2527521)*
glucanase			
BN869_T00009871_1	putative endo-beta-1,4-glucanase D	*1.2 (0.918)*	**6.47 (3.758E-10)**
Hydrolases_general			
BN869_T00000016_1	glycoside hydrolase family 28 protein	*0.59 (0.852)*	**6.11 (0.0097954)**
BN869_T00000899_1	glycoside hydrolase family 114 protein	*0.98 (0.986)*	**7.77 (2.472E-07)**
BN869_T00003909_1	related to glycosyl hydrolase	*0.31 (0.432)*	**26.53 (4.119E-19)**
BN869_T00004834_1	glycoside hydrolase family 115 protein	*1.15 (0.954)*	**5.01 (0.0493978)**
BN869_T00005806_1	glycoside hydrolase family 81 protein	*1.09 (0.76)*	**4.99 (2.773E-14)**
BN869_T00008474_1	hydrolase, alpha/beta fold family	*0.91 (0.887)*	**33.92 (3.19E-188)**
BN869_T00008724_1	glycoside hydrolase family 89 protein	*0.65 (0.822)*	**5.32 (8.415E-09)**
BN869_T00009923_1	glycosyl hydrolase family 12	*0.59 (0.852)*	**4.48 (0.0103006)**
BN869_T00010029_1	glycoside hydrolase family 31 protein	*0.59 (0.852)*	**6.55 (0.0112524)**
BN869_T00013149_1	glycoside hydrolase family 61 protein	**35.71 (0.0009)**	*1.23 (0.7037736)*
BN869_T00014078_1	alpha beta hydrolase fold protein	**18.52 (3.79E-12)**	**3.57 (6.782E-25)**

Table 3. *F. graminearum* genes associated with phosphate starvation are induced before and after being challenged by *C. rosea*. Fold change values in bold type are significant at FDR p-value<0.05 while italicized fold change values are not (p-value >0.05).

Gene	Annotation	**Before Contact** Fold Change FDR (p-value)	**After Contact** Fold Change FDR (p-value)
FGRAMPH1_01G01877	betaine lipid synthase (*BTA1*)	**110.03 (0)**	*1.16* (0.5)
FGRAMPH1_01G08015	sodium/phosphate co-transporter	**2.92 (0)**	*-1.32* (0.063)
FGRAMPH1_01G12109	lipid phosphatidate phosphatase	**6.80 (8.7E-15)**	**21.83 (0)**
FGRAMPH1_01G12703	acid phosphatase (*PHO5*-like)	**4.58 (0)**	**-1.52 (0.007)**
FGRAMPH1_01G12793	acid phosphatase (*PHO5*-like)	**4.03 (4.8E-9)**	**18.92 (0)**
FGRAMPH1_01G13431	plasma membrane transporter importing glycerol-3-phosphate and phospholipids	**4.05 (0)**	**1.43 (0.004)**
FGRAMPH1_01G15463	acid phosphatase	**32.98 (0)**	**-2.02 (3.7E-5)**
FGRAMPH1_01G19107	acid phosphatase	**8.99 (0)**	*1.02* (0.99)
FGRAMPH1_01G25367	acid phosphatase	**12.40 (0)**	**-2.25 (6.7E-14)**
FGRAMPH1_01G25919	high-affinity phosphate transporter	**16.84 (0)**	**-1.31 (0.034)**
FGRAMPH1_01G04877	lipid phosphate phosphatase 2	*1.19* (0.27)	**7.18 (0)**
FGRAMPH1_01G22711	alkaline phosphatase	**115.39 (0)**	**-1.84 (0.018)**

Table 4. **List of upregulated MFS type transporter homolog transcripts at p value <0.05 and their classification.** Significant expression value are given in bold and those upregulated in both BC and AC are shaded with light grey.

		BC		AC		
No	Transcript ID	Fold Change	p-value	Fold Change	p-value	MFS Family
1	BN869_T00004802_1	**8.06**	*0.00093*	*1.20*	*0.00101*	**2.A.1.1** (The Sugar Porter (SP) Family)
2	BN869_T00009898_1	**5.85**	*4E-20*	**5.89**	*4E-121*	
3	BN869_T00000518_1	**4.37**	*4.2E-05*	*0.75*	*1.6E-18*	
4	BN869_T00013994_1	**3.16**	*1.1E-11*	**2.63**	*7.2E-67*	
5	BN869_T00002616_1	*1.60*	*3.4E-12*	**2.73**	*0*	
6	BN869_T00011473_1	*1.08*	*0.91019*	**3.07**	*0.04738*	
7	BN869_T00010393_1	*0.85*	*0.85195*	**7.86**	*1.2E-05*	
8	BN869_T00002201_1	*0.79*	*0.20142*	**4.24**	*6.3E-80*	
9	BN869_T00010022_1	*0.79*	*0.53635*	**2.56**	*1.6E-18*	
10	BN869_T00000891_1	*0.77*	*0.35862*	**5.96**	*3.9E-54*	
11	BN869_T00005632_1	*0.77*	*0.00727*	**2.49**	*0*	
12	BN869_T00012137_1	*0.67*	*0.40332*	**2.50**	*3E-11*	
13	BN869_T00011842_1	*0.56*	*0.48441*	**6.41**	*7.1E-05*	
14	BN869_T00013528_1	*0.53*	*0.00892*	**2.70**	*4.3E-20*	
15	BN869_T00010377_1	*0.39*	*0.00012*	**3.28**	*2.8E-27*	
16	BN869_T00008572_1	*0.38*	*0.02242*	**2.68**	*1E-05*	
17	BN869_T00012857_1	*0.15*	*1.4E-23*	**2.54**	*1E-125*	
18	BN869_T00005309_1	**2.60**	*0.02687*	*0.19*	*4.7E-08*	**2.A.1.12.2** (The lactate/pyruvate:H+ symporter)
19	BN869_T00005193_1	**2.49**	*0.00319*	**2.17**	*2.7E-15*	
20	BN869_T00000934_1	**2.46**	*1.2E-09*	*1.56*	*0.00031*	
21	BN869_T00004864_1	*1.30*	*0.70339*	**3.47**	*0.01532*	
22	BN869_T00013019_1	**5.99**	*0.19126*	*0.26*	*1.1E-05*	**2.A.1.14** (The Anion:Cation Symporter (ACS) Family)
23	BN869_T00006489_1	**4.03**	*8.9E-07*	*0.40*	*0.00159*	
24	BN869_T00002489_1	**2.58**	*2.5E-05*	*0.74*	*0.08715*	
25	BN869_T00012163_1	*1.16*	*0.80486*	**5.11**	*0.00066*	
26	BN869_T00008448_1	*0.60*	*0.4373*	**2.49**	*0.00037*	
27	BN869_T00013493_1	*0.56*	*0.36767*	**2.93**	*0.00136*	
28	BN869_T00001004_1	*0.49*	*0.50626*	**5.49**	*0.00164*	
29	BN869_T00009316_1	*0.39*	*0.05858*	**2.61**	*6.1E-07*	
30	BN869_T00012452_1	*0.33*	*8.3E-06*	**2.75**	*3.5E-09*	
31	BN869_T00007109_1	*0.29*	*0.04039*	**2.56**	*9E-20*	
32	BN869_T00008582_1	*0.26*	*0.0004*	**2.57**	*1E-07*	
33	BN869_T00006919_1	*0.25*	*0.33948*	**12.63**	*2.2E-06*	
34	BN869_T00000901_1	*0.25*	*4.4E-06*	**3.52**	*7.1E-10*	
35	BN869_T00004349_1	*0.22*	*0.04772*	**4.65**	*2.3E-09*	
36	BN869_T00000978_1	*0.16*	*0.15304*	**3.80**	*0.04478*	
37	BN869_T00007234_1	**125.00**	*8E-103*	**56.35**	*1.4E-92*	**2.A.1.2** (The Drug:H+
38	BN869_T00000794_1	**4.22**	*2.2E-17*	0.49	3.6E-52	

39	BN869_T00004654_1	**2.90**	*4.3E-17*	0.54	1.1E-45	Antiporter-1 (12 Spanner) (DHA1) Family)
40	BN869_T00001547_1	**2.48**	*1.9E-10*	0.47	1.8E-74	
41	BN869_T00014038_1	*3.23*	*0.1365*	**2.60**	*0.02074*	
42	BN869_T00008955_1	*2.71*	*0.13085*	**2.01**	*4.9E-05*	
43	BN869_T00005769_1	*0.98*	*0.99265*	**2.53**	*0.02697*	
44	BN869_T00005588_1	*0.52*	*0.53732*	**2.87**	*0.00474*	
45	BN869_T00002203_1	*0.44*	*0.00023*	**2.86**	*4.5E-31*	
46	BN869_T00007594_1	**14.29**	*2.4E-31*	*0.61*	*2.3E-10*	**2.A.1.3** (The Drug:H+ Antiporter-2 (14 Spanner) (DHA2) – most toxin efflux MFS belong to this family)
47	BN869_T00013211_1	**12.99**	*9.5E-05*	*1.46*	*0.31936*	
48	BN869_T00013338_1	**3.83**	*0.01993*	*0.49*	*2E-212*	
49	BN869_T00010959_1	**2.74**	*1.9E-17*	*0.10*	*8E-307*	
50	BN869_T00005590_1	**2.72**	9.5E-08	*0.85*	*0.33959*	
51	BN869_T00009641_1	**2.68**	*0.04434*	*0.51*	*2E-06*	
52	BN869_T00009232_1	**2.65**	*1.3E-08*	*0.97*	*0.74365*	
53	BN869_T00006965_1	**2.59**	*2.5E-06*	*0.78*	*0.11555*	
54	BN869_T00008098_1	*1.04*	*0.92697*	**2.54**	*3.9E-09*	
55	BN869_T00011832_1	*0.91*	*0.89723*	**3.29**	*4.5E-33*	
56	BN869_T00005651_1	*0.84*	*0.77451*	**3.07**	*1.8E-17*	
57	BN869_T00007791_1	*0.16*	*0.28372*	**3.69**	*0.01659*	
58	BN869_T00002816_1	**4.93**	*6.7E-14*	*0.71*	*3.8E-07*	**2.A.1.7** (Uncharacterized protein)
59	BN869_T00010994_1	**4.31**	*0.01481*	*0.77*	*0.1215*	
60	BN869_T00012492_1	*0.87*	*0.90491*	**3.87**	*8.3E-07*	
61	BN869_T00006371_1	*0.73*	*0.16305*	**2.71**	*1.1E-18*	
62	BN869_T00005531_1	*1.11*	*0.45855*	**4.72**	*5E-151*	Unknown family
63	BN869_T00006259_1	*1.61*	*6.1E-10*	**2.50**	*7E-156*	

FIGURE LEGENDS

Fig. 1. Differential regulation of *C. rosea* strain AMC941 transcripts during confrontation with F. graminearum. Volcano plots of differential gene expression arising from *C. rosea vs F. graminearum* co-culture relative to *C. rosea* mono-culture **A,** before the two colonies touched each other and **B,** after the two colonies touched each other. Volcano plots were obtained using DESeq2 software.

Fig. 2. Validation of RNAseq results by qPCR. Results arising for a number of selected unchanged, upregulated and downregulated transcripts are shown. **A,** BC **-** before contact and **B,** AC **-** after contact. Transcript ID description **Cr07230** - BN869_T00007230_1, **Cr07231** - BN869_T00007231_1, **Cr07232** - BN869_T00007232_1, **Cr07233** - BN869_T00007233_1, **Cr07234 -** BN869_T00007234_1, **Cr07235** - BN869_T00007235_1, **Cr07236 -** BN869_T00007236_1, **Cr07657 -** BN869_T00007657_1, **Cr08207 -** BN869_T00008207_1, **Cr05310 -** BN869_T00005310_1, **Cr04860 -** BN869_T00004860_1, **Cr10434 -** BN869_T00010434_1 and **Cr08191 -** BN869_T00008191_1. RNAseq outcomes are represented by black bars, qPCR outcomes are represented by open bars.

Fig. 3. RNAseq expression results for *F. graminearum* trichothecene gene cluster before contact with *C. rosea*, with validation using ddPCR. Fungal *ßtub* and *EF1α* genes were used as internal controls for normalization of transcripts. Three biological replicates of each treatment were assayed. Only *TRI8*, *TRI4* and *TRI1* were assayed by ddPCR. RNAseq outcomes are represented with black bars, ddPCR outcomes are represented by grey bars.

Fig. 4. Comparative expression profile of top 100 upregulated transcripts. A, *C. rosea* and **B,** *F. graminearum,* before contact (log2FC-BC) and after contact (log2FC-AC). Only ten

transcripts were upregulated in both stages. List of transcripts and their expression profile is given in Table S1.

Fig. 5. Expression of a *C. rosea* polyketide containing gene cluster by RNAseq with validation by qPCR. **A,** before contact and **B,** after contact. *C. rosea ßAct* and *EF1α* genes were used as internal controls for normalization of transcripts. Transcript ID description **Cr12005** - BN869_T00012005_1, **Cr12006** - BN869_T00012006_1, **Cr12007** - BN869_T00012007_1, **Cr12008** - BN869_T00012008_1, **Cr12009 -** BN869_T00012009_1, **Cr12010** - BN869_T00012010_1, **Cr12011 -** BN869_T00012011_1 and **Cr12012** - BN869_T00012012_1. RNAseq outcomes are represented by black bars, qPCR validation is represented by open bars.

Fig. 6. Metabolic profile of *C. rosea* and *F. graminearum* strain after seven day co-culture. Heat map comparison of autoscaled discriminatory variables representing secondary metabolites that accumulated by the AC stage (day 7) between *C. rosea* strain ACM941 (Cr) and *F. graminearum* strain Fg3639 (Fg) monocultures and their respective interaction zones in co-culture (Cr-I and Fg-I). Representative metabolite variables expressed as retention time_mass/charge ratio (RT_*m/z*) or by a designation (15ADON-3G = 15-ADON-3-Glc; TDO = trichodimerol; TDO-associated = trichodimerol associated; TRI-associated = trichothecene associated). Black arrow included to highlight 15-ADON and purple arrow for 15-ADON-3-Glc.

Fig. 7. Representative *C. rosea* secondary metabolites expressed in monoculture and co-culture experiments (Cr = *C. rosea* monoculture; Cr-I = co-culture *C. rosea* interaction zone; Fg = *F. graminearum* monoculture; Fg-I = co-culture *F. graminearum* interaction zone). **A,** Molecular structure, formula, and mass of trichodimerol. **B,** ANOVA box plots of normalizaed peak area of trichodimerol $[M+H]^+$ pseudomolecular ion (mass error: -0.32 ppm) observed at 5d

(BC) and 7d (AC). **C,** Molecular structure, formula, and mass of TMC-151E. **D,** ANOVA box plots of normalizaed peak area of TMC-151E $[M+Na]^+$ pseudomolecular ion (mass error: 0.29 ppm) observed at 5d (BC) and 7d (AC).

Fig. 8. Observed trends in 15-ADON and 15-ADON-3-Glc accumulation in monoculture and co-culture experiments (Cr = *C. rosea* monoculture; Cr-I = co-culture *C. rosea* interaction zone; Fg = *F. graminearum* monoculture; Fg-I = co-culture *F. graminearum* interaction zone). **A,** Molecular structure, formula, and mass of 15-ADON. **B**, ANOVA box plots of normalizaed peak area of 15-ADON $[M+Na]^+$ pseudomolecular ion (mass error: -1.63 ppm) observed at 5d (BC) and 7d (AC). **C,** Molecular structure, formula, and mass of 15-ADON-3-Glc. **D,** ANOVA box plots of normalizaed peak area of 15-ADON-3-Glc $[M+Na]^+$ pseudomolecular ion (mass error: -0.50 ppm) observed at 5d (BC) and 7d (AC).

Supplemental Figues:

Supplemental Figures S1-S5 are included in the file entitled ‘Supplemental Figures.pdf’.

Supplemental Tables:

Supplemental Tables S1-S8 are included in the file entitled ‘Supplemental Tables.xls’.

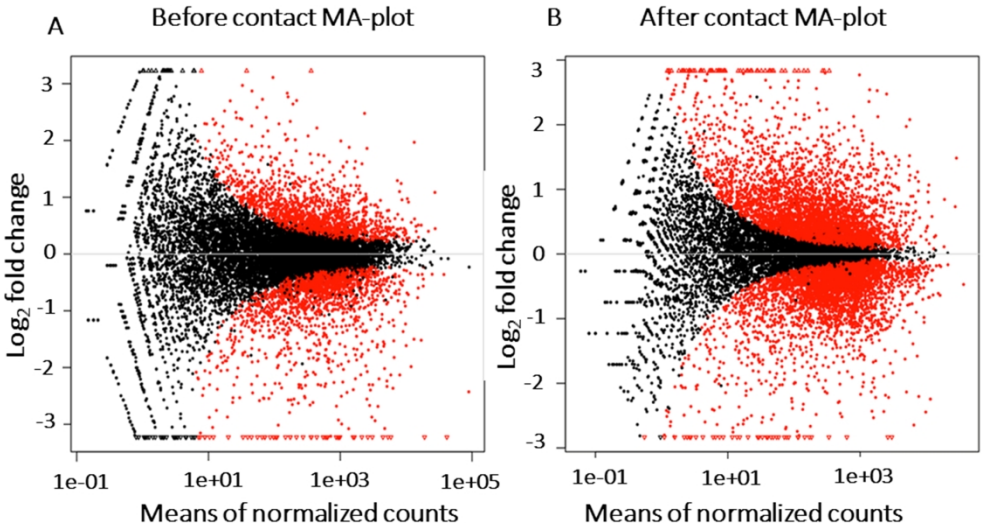

Figure 1

177x95mm (768 x 768 DPI)

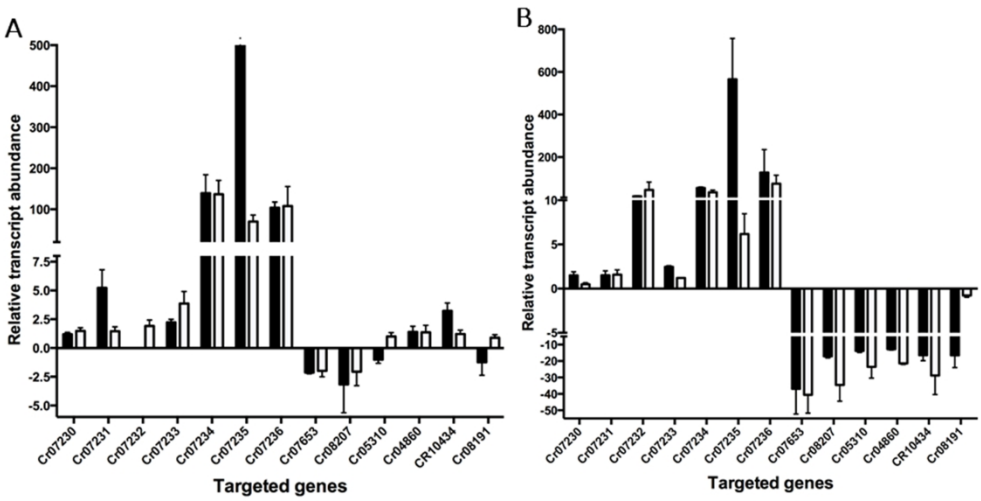
A
B
Relative transcript abundance
Targeted genes
Cr07230
Cr07231
Cr07232
Cr07233
Cr07234
Cr07235
Cr07236
Cr07653
Cr08207
Cr05310
Cr04860
CR10434
Cr08191

Figure 2

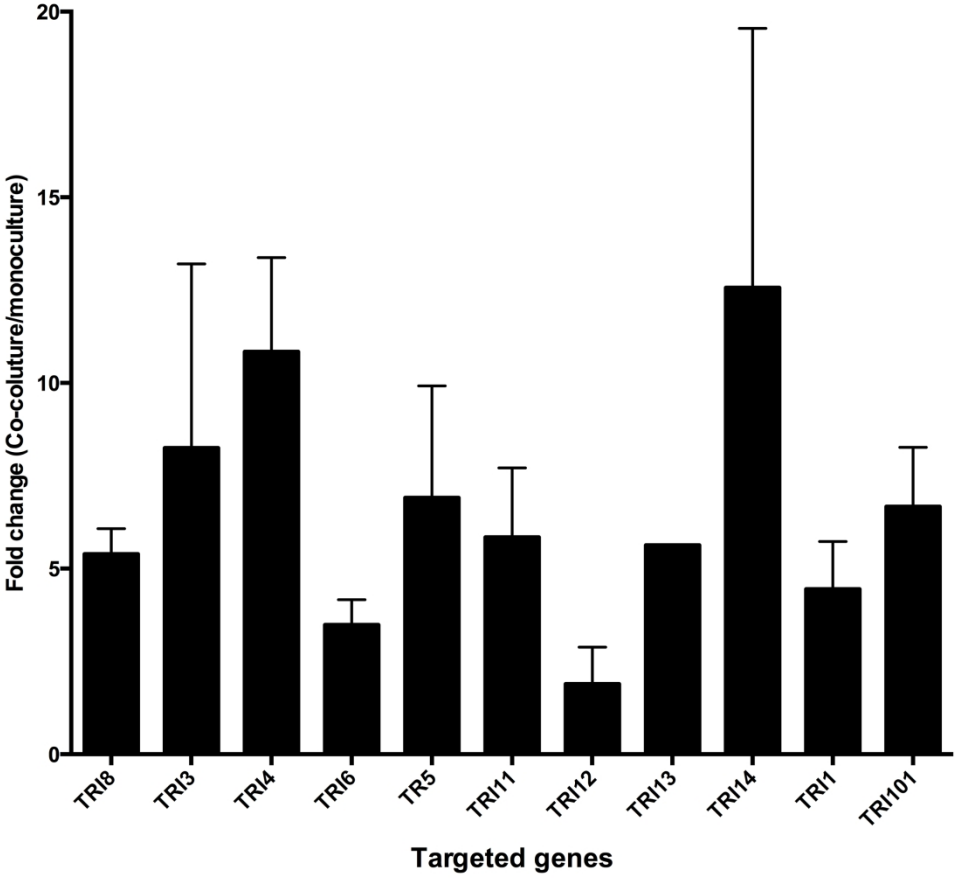

Figure 3

88x79mm (768 x 768 DPI)

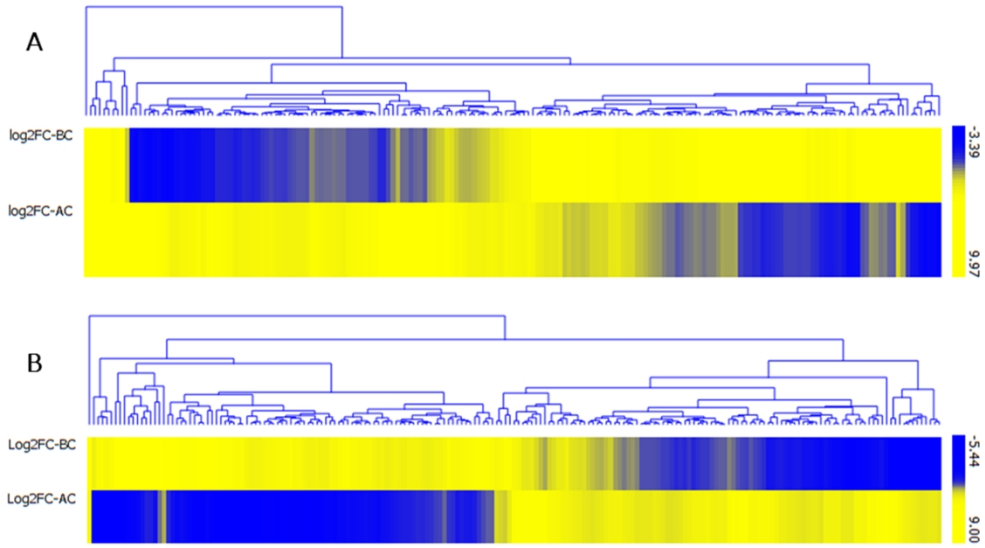

Figure 4

177x102mm (768 x 768 DPI)

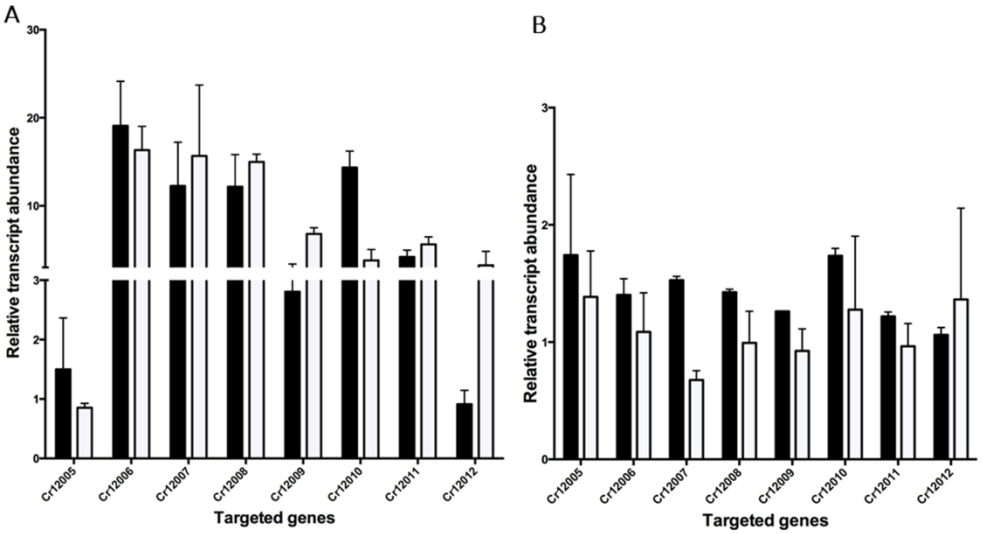

Figure 5

177x95mm (768 x 768 DPI)

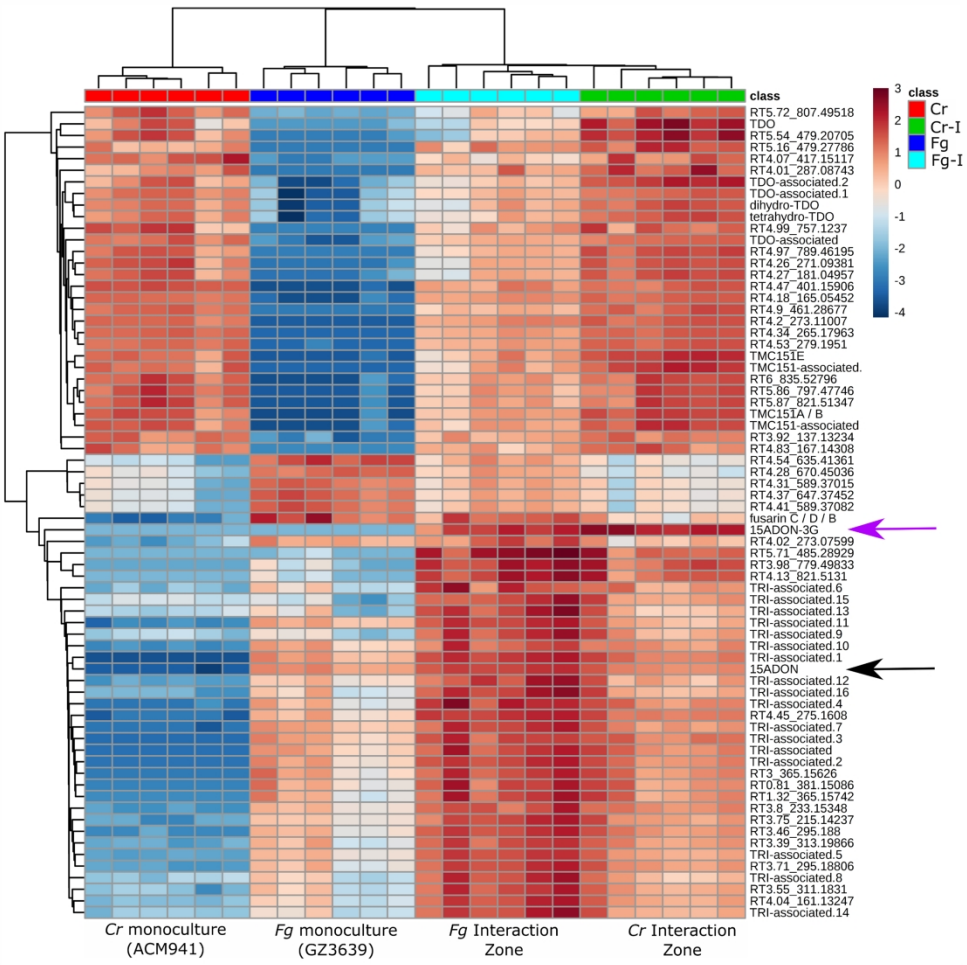

Figure 6

177x173mm (768 x 768 DPI)

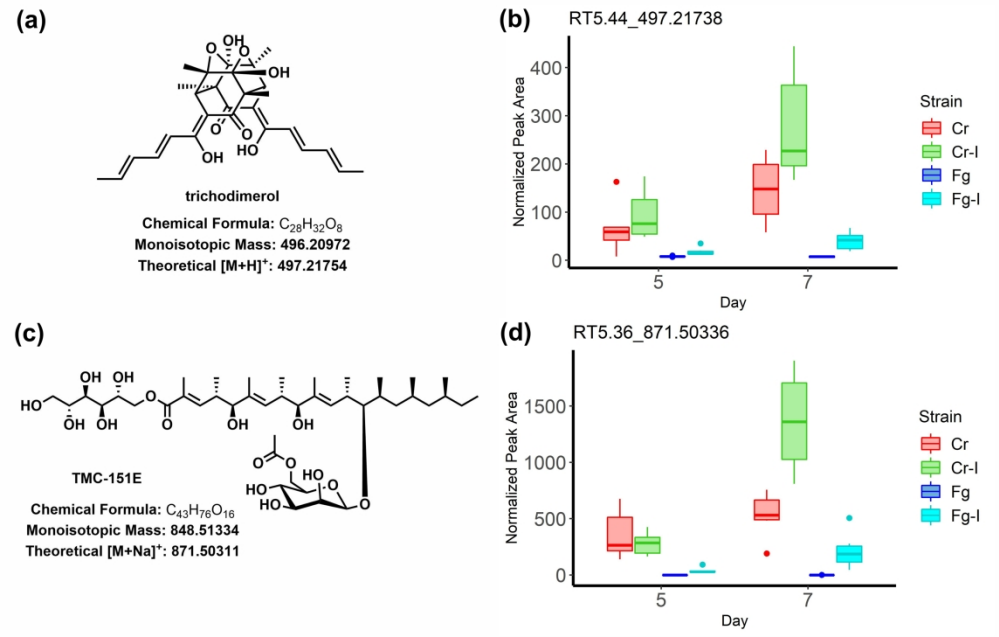

Figure 7

177x113mm (768 x 768 DPI)

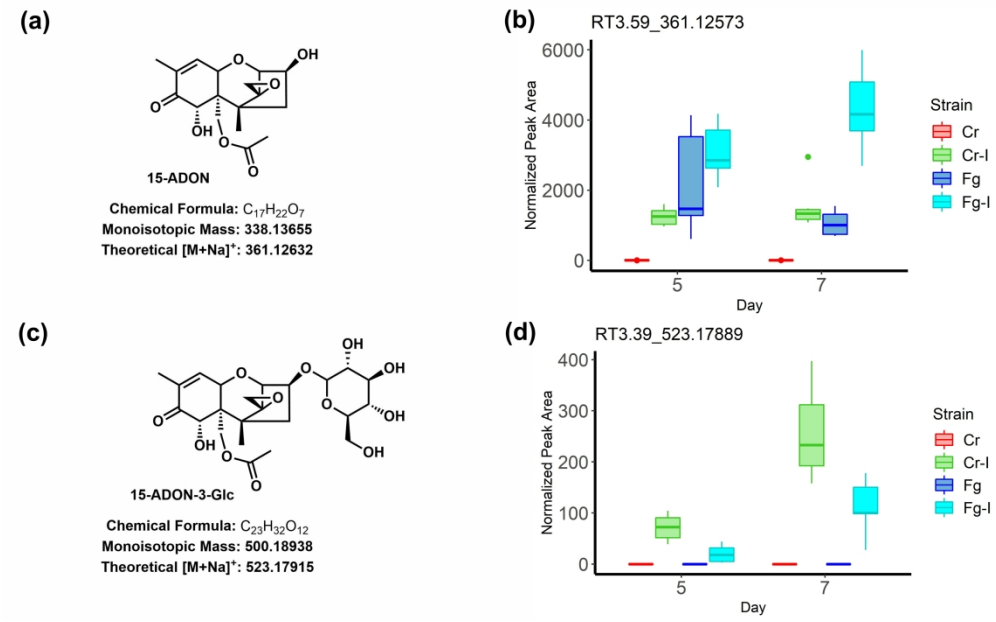

Figure 8

177x110mm (768 x 768 DPI)

Transcriptomic and exometabolomic profiling reveals antagonistic and defensive modes of *Clonostachys rosea* action against *Fusarium graminearum*

Zerihun A. Demissie[1], Thomas Witte[2], Kelly A. Robinson[1], Amanda Sproule[2], Simon J. Foote[3], Anne Johnston[2], Linda J. HarriS[2], David P. Overy[2] and Michele C. Loewen[1,4,5*]

Supplemental Figures S1 – S5

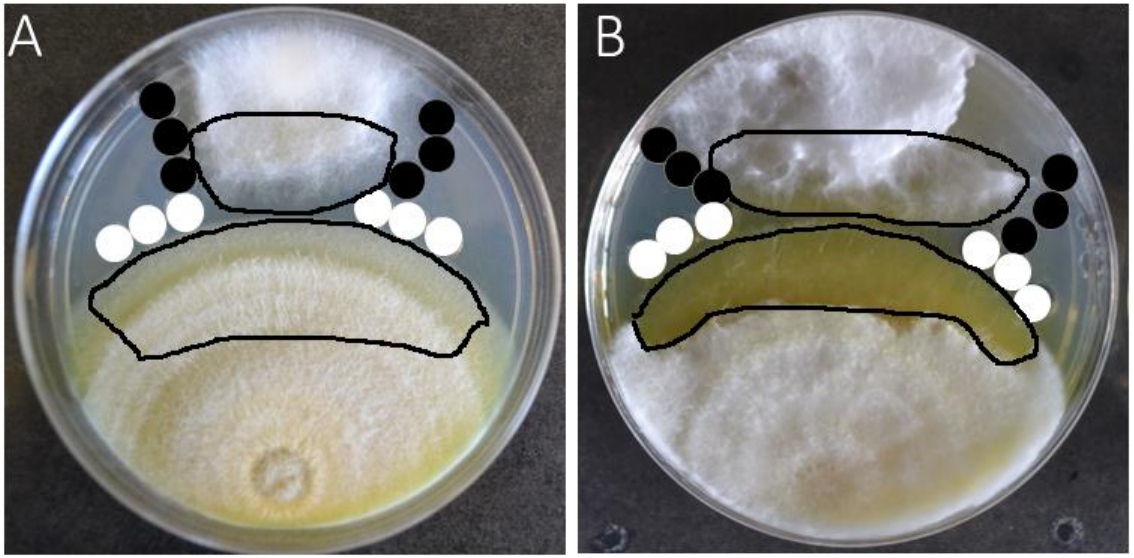

Fig. S1 Representative photos of *C. rosea* and *F. graminearum* interaction on plate. **A**, BC and **B**, AC. Agar plugs sampled for *C. rosea* metabolite extraction were represented by white circles while that of *F. graminearum* were represented by black circles. Area scrapped for RNA extraction is encircled.

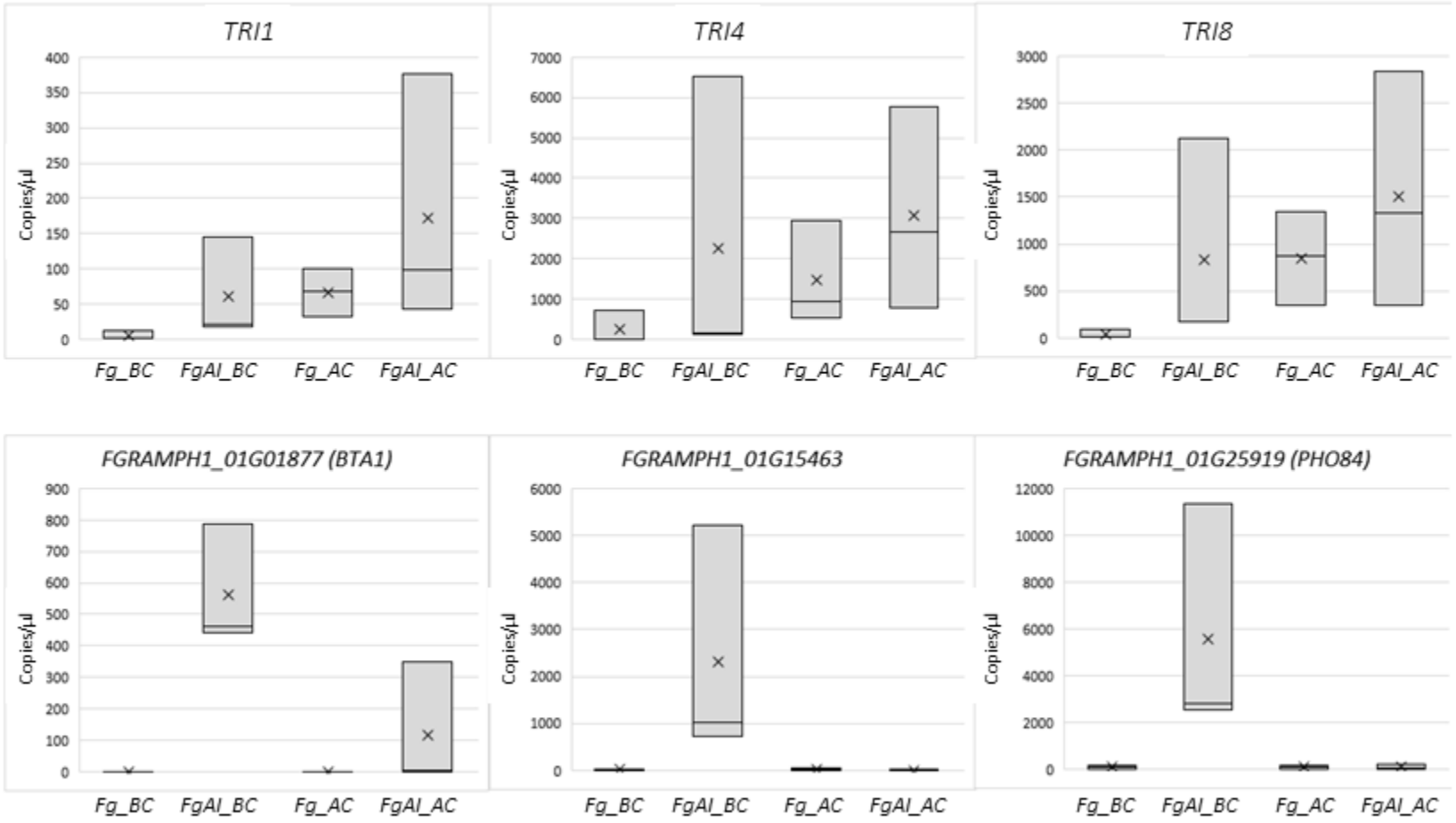

Fig. S2 Validation of selected *TRI* and phosphate starvation related *F. graminearum* RNAseq result by ddPCR. AC = after contact; BC = before contact; *Fg* = *F. graminearum* monoculture; *FgAI* = *F. graminearum* co-cultured with *C. rosea*.

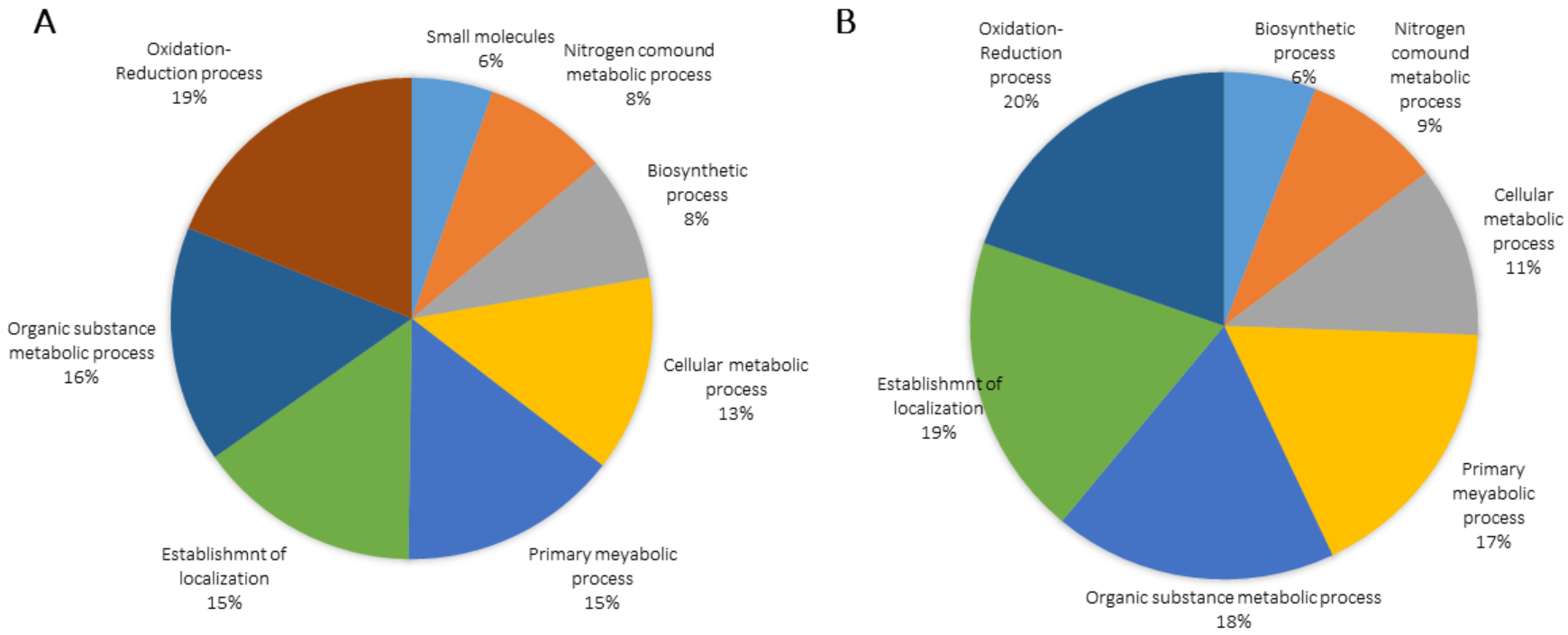

Fig. S3 Gene ontology analysis of biological process classification of *C. rosea* transcripts with ≥2.5 fold expression changes. **A,** before contact and **B**, after contact.

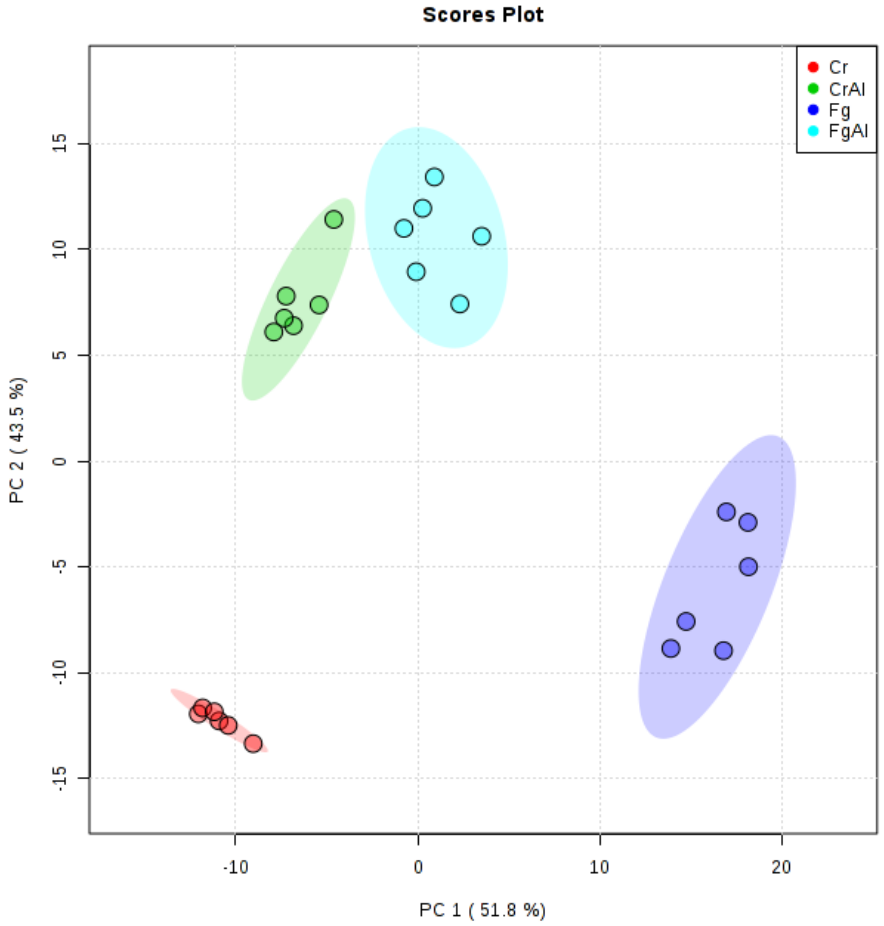

Fig. S4 PCA of metabolites isolated after contact (AC). Cr = *C. rosea* monoculture; CrAI = *C. rosea* interaction zone; FgAI = *F. graminearum* interaction zone; Fg = *F. graminearum* monoculture.

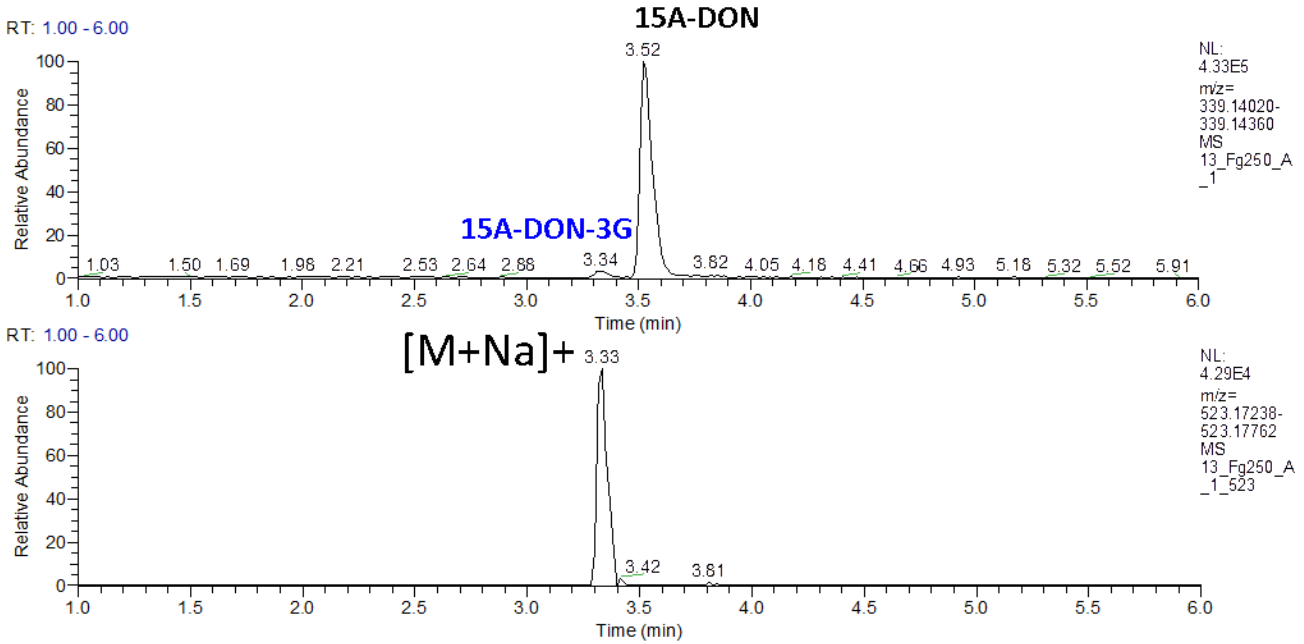

Fig. S5 Glycosylation of exogenously applied 15-ADON by *C. rosea*. Top panel, extracted ion chromatogram of mass range (*m/z* 339.14271 – 339.14611) representing 15-ADON $[M+H]^+$ and 15-ADON-Glc [15-ADON fragment+H]$^+$ ions, with metabolites arising from *C. rosea* extracts following challenge with 15-ADON. Extracted ion chromatogram of mass range (*m/z* 523.17238 – 523.17762) representing 15-ADON-glycoside $[M+Na]^+$ ions observed from *C. rosea* culture extracts when challenged with 15-ADON.